Remote Sensing of Environment 133 (2013) 71–84

Contents lists available at SciVerse ScienceDirect

Remote Sensing of Environment

journal homepage: www.elsevier.com/locate/rse

Spatial and temporal validation of the MODIS LAI and FPAR products across a boreal forest wildfire chronosequence

Shawn P. Serbin *, Douglas E. Ahl [1], Stith T. Gower

Department of Forest and Wildlife Ecology, 226 Russell Labs, 1630 Linden Dr., University of Wisconsin, Madison, WI 53706, United States

ARTICLE INFO

Article history:
Received 15 February 2011
Received in revised form 15 January 2013
Accepted 26 January 2013
Available online xxxx

Keywords:
MODIS
LAI
FPAR
Phenology
Boreal forest
Understory vegetation
Leaf area index
EOS land validation core sites

ABSTRACT

The leaf area index (LAI) and fraction of photosynthetically active radiation (FPAR) absorbed by the vegetation are key biophysical measures of canopy foliage area and light harvesting potential. Accurately quantifying these properties is important for characterizing the dynamics of mass and energy exchanges between vegetation and the atmosphere. The overall objective of this research was to validate the spatial and temporal performance of the MODIS LAI/FPAR products for a boreal forest landscape in northern Manitoba, Canada. We examined both the MODIS collection 4 (C4) and updated collection 5 (C5) versions over a multiyear period (2004 to 2006) and spatially across seven different-aged forests originating from wildfire and ranging in age from 1- to 154-years-old. We made optical measurements of LAI and FPAR, which were empirically scaled to high-resolution imagery (ASTER; 15–30 m pixel size) to derive detailed reference LAI and FPAR maps. These maps were then aggregated to MODIS resolution (i.e. 1 km) for comparison. We characterized the temporal accuracy of the MODIS products using repeat measurements of LAI and FPAR, and through comparisons with continuously operating measurements of canopy light interception.

MODIS captured the general phenological trajectory of these aggrading forests, however the MODIS LAI and FPAR products overestimated and underestimated the LAI and FPAR for the youngest and oldest sites, respectively. In addition, MODIS displayed larger seasonal variation in LAI and FPAR compared to field measurements for the needle-leaf evergreen dominated sites. The peak growing season difference between MODIS and spatially aggregated ASTER reference values of LAI and FPAR decreased significantly by 69% and 55%, respectively, for the updated C5 versus the previous C4 LAI/FPAR products. The overall uncertainty (i.e. RMSE) in the MODIS LAI retrievals decreased from 1.6 (C4) to 0.63 m^2 m^{-2} (C5) and from 0.20 (C4) to 0.07 (C5) for FPAR. The incorporation of understory vegetation into the validation of the MODIS products yielded significantly higher agreement between observed and MODIS values, likely due to the relatively open canopy architecture and abundant understory found within boreal forests.

1. Introduction

Atmospheric concentrations of carbon dioxide (CO_2) have been increasing in recent decades (Hofmann et al., 2006; Raupach et al., 2007) with implications for global climate forcing and feedbacks (Cox et al., 2000; Lacis et al., 2010). Contemporary observations suggest a global pattern of steady warming during the past three decades (Hansen et al., 2006), and average surface temperatures in North America are projected to increase by as much as 1–6 °C in the next half century (IPCC, 2007). The northern high latitude ecosystems, including boreal forests, have experienced greater warming than other biomes in recent decades, particularly during the winter and spring (Lucht et al., 2002), and this trend is predicted to continue (ACIA, 2004; Sanderson et al., 2011). Increased climate warming can affect canopy dynamics such as the leaf area index (LAI; m^2 m^{-2} per horizontal datum), fraction of photosynthetically active radiation (FPAR) absorbed by the vegetation, and canopy phenology, which are key determinants of carbon uptake by vegetation (Barr et al., 2004; Bonan, 1993; Piao et al., 2007; Richardson et al., 2010; Sellers et al., 1997a). Warmer temperatures may increase the growing season length, which could enhance the carbon uptake of temperature-constrained boreal forests (Barr et al., 2007; Keeling et al., 1996; Myneni et al., 1997; Randerson et al., 1999). However, complex land-atmosphere feedbacks and altered disturbance regimes may also produce strong limitations to any potential enhancement of carbon sequestration (e.g. Angert et al., 2005; Goetz et al., 2005; Kurz et al., 2008; Piao et al., 2008; Turetsky et al., 2011).

Boreal forests are a particularly important component of the global carbon cycle because they encompasses almost 30% of the Earth's total forested area and contain a significant percentage of the total terrestrial carbon in the soil (~25–31%) and aboveground vegetation (~26%, Gower et al., 1997; McGuire et al., 2002; Tarnocai et al., 2009). Increased wildfire over the last several decades, due in part to a warmer climate (Gillett et al., 2004; Kasischke & Turetsky, 2006; Stocks et al., 2003),

* Corresponding author. Tel.: +1 608 556 2956; fax: +1 608 262 9922.
E-mail address: serbin@wisc.edu (S.P. Serbin).
[1] Current Address: Energy Center of Wisconsin, 455 Science Drive, Suite 200, Madison, WI 53711, United States.

0034-4257/$ – see front matter © 2013 Elsevier Inc. All rights reserved.
http://dx.doi.org/10.1016/j.rse.2013.01.022

has changed the net biome production of the boreal forests in Saskatchewan and Manitoba from a weak carbon sink to a modest carbon source (Bond-Lamberty et al., 2007). Increased fire frequency shortens the recovery period between fires (Johnstone & Chapin, 2006), which may influence forest successional trajectories. In addition, fire extent has been increasing (Kasischke & Turetsky, 2006), a trend that is expected to continue (Flannigan et al., 2005; Stocks et al., 1998). Furthermore, wildfire disturbances directly influence boreal forest structure, composition, phenology, energy fluxes, and productivity (Amiro, 2001; Amiro et al., 2006; Bond-Lamberty et al., 2007; Goulden et al., 2011; Johnstone & Kasischke, 2005; Serbin et al., 2009), which influences seasonal patterns of satellite reflectance (Goetz et al., 2006; Peckham et al., 2008; Serbin et al., 2009; Steinberg et al., 2006). This result is particularly important for the accurate monitoring and attribution of vegetation changes in response to the combined influences of global change and altered disturbance regimes.

Species composition and structure of the boreal forest landscape is highly variable due to the impacts of topography and drainage, as well as the frequent occurrence of wildfire. The canopy structure can range from bryophyte and shrub dominated early successional forests, to mixed tree species in mid-successional stands, to evergreen (pine and spruce), broad-leaf deciduous forests (e.g. aspen) or needle-leaf deciduous forests (Gower & Richards, 1991; Gower et al., 1997; Viereck et al., 1983). This complex and dynamic architecture makes accurately quantifying the canopy dynamics of boreal forests challenging (Chen et al., 1997; Kucharik et al., 1999; Miller et al., 1997; Serbin et al., 2009), especially with moderate-resolution sensors such as the MODerate resolution Imaging Spectrometer (MODIS), which observe a complex vegetation mosaic within individual pixels (Cohen et al., 2006; Garrigues et al., 2006; Tan et al., 2005; Wang et al., 2004). Thus, there is a great need to better understand how fire influences satellite estimates of LAI and FPAR, including the retrievals during succession and changes in forest community composition, as well as capturing the seasonality in these parameters. This is particularly important for the development of reliable spatial data that are critical inputs for terrestrial biogeochemical models that require these data to simulate carbon exchange (e.g. Running et al., 2004).

Several research groups have observed seasonal and/or interannual variation in canopy phenology of global boreal forests using remotely sensed data. The changes have been attributed to climate (e.g. de Beurs & Henebry, 2010; Myneni et al., 1997; Shabanov et al., 2002) or increased fire frequency (e.g. Goetz et al., 2006; Peckham et al., 2008). In this study, we assessed the performance of the MODIS MOD15 LAI and FPAR products (Knyazikhin et al., 1998; Shabanov et al., 2005; Yang et al., 2006a) for a boreal forest landscape in northern Manitoba, Canada. The overall goal of this research was to validate the spatial and temporal performance and retrieval characteristics of these products across multiple years (i.e. 2004–2006) in boreal forests of differing time since stand-initiating fire. We focused on this region because it is the location of the BOREAS Northern Study Area (NSA), and we have conducted research in this area for two decades. Specific objectives were to (1) compare field- and MODIS-based estimates of FPAR and LAI for the seven different-aged sites comprising the wildfire chronosequence; (2) examine seasonal variability in MODIS retrievals across the burn sites in relation to successional stage and forest composition; (3) examine the influence of understory vegetation on the MODIS biophysical retrievals; (4) investigate potential reasons for discrepancies between MODIS and observed values of LAI and FPAR.

2. Methods

2.1. Description of the study area

The research was conducted near Thompson, Manitoba, Canada, from the spring of 2004 through the fall of 2006. This region includes the Boreal Ecosystem and Atmospheric Study (BOREAS) — Northern Study Area (55° 53′ N, 98° 20′ W), which is a NASA Earth Observing System (EOS) core validation site (Sellers et al., 1997b). Wildfire is the dominant disturbance in this region. The terrain is relatively gentle, and the elevation ranges from about 178 m to 350 m above sea level. The mean annual air temperature was −1.64 °C, 0.44 °C, and −0.81 °C for 2004, 2005, and 2006, respectively. The mean (2004–2006) air temperatures in January and July were −24 °C and 18 °C, respectively. Annual precipitation averaged 604 mm (±263.8 mm).

The seven sites in this study were part of a wildfire chronosequence study (Bond-Lamberty et al., 2004, 2002; Serbin et al., 2009) that originated from stand replacing wildfires that occurred in ~1850, ~1930, 1964, 1981, 1989, 1994 and 2003 (Fig. 1). At the beginning of the study (2004) the sites ranged in age from 1 to 154 years-old. The chronosequence encompassed a broad range of age classes, basal area, stocking density, and canopy closure (Table 1) that are the result of the interaction of burn severity, topography, and edaphic conditions (Bond-Lamberty et al., 2004, 2002; Serbin et al., 2009). Common overstory species were black spruce (*Picea mariana*), jack pine (*Pinus banksiana*), trembling aspen (*Populus tremuloides*) and willow (*Salix*, spp.); other less common tree species included paper birch (*Betula papyrifera*) tamarack (*Larix laricina*) and balsam poplar (*Populus balsamifera*). Ground cover species varied with drainage, and included feather mosses (usually *Pleurozium*, *Ptilium*, *Hylocomium*, spp.) and reindeer lichen (*Cladina*, spp.) for well-drained areas, while the poorly-drained areas contained sphagnum mosses (*Sphagnum* spp.) with an understory of Labrador tea (*Ledum groenlandicum*) and bog birch (*Betula glandulosa*). Briefly, in this study we define a "site" as each burn scar, defined by the historical burn perimeter (e.g. 2003 burn site, see Fig. 1), while a "stand" is defined as a particular location within a site that contains similar drainage and vegetation community characteristics (e.g. well- versus poorly-drained stands).

The dominant vegetation at the youngest site (2003 burn) included prickly rose (*Rosa acicularis*), fireweed (*Epilobium angustifolium*), and horsetail (*Equisetum*, spp.) with lesser amounts of labrador tea, willow (*Salix*, spp.) and periodic black spruce seedlings; a few small pockets of unburned black spruce trees were also present. The composition of the early successional sites (1994 and 1989 burns) was largely willow, jack pine, and aspen in the overstory, with fireweed, prickly rose, labrador tea, and blueberry (*Vaccinium myrtilloides*) found in the understory. Mid successional sites (1981–1964) contained deciduous and coniferous species in the overstory, with an understory of cranberry (*Vaccinium vitis-idaea*), bearberry (*Arctostaphylos uva ursi*), labrador tea and bog birch. Black spruce and a few jack pine, aspen, balsam poplar and tamarack largely dominated the canopy of the oldest 1930 and 1850 burn sites. Common understory shrubs included labrador tea, willow, and green alder (*Alnus crispa*). Feather moss was the dominant ground cover in the upland areas, and sphagnum was the dominant ground cover on wet, poorly-drained areas.

2.2. MODIS products

The MODIS MOD15A2 LAI/FPAR product is produced globally at a 1 km resolution over a sinusoidal grid divided into ~1200×1200 km tiles (Yang et al., 2006a). The algorithm generates daily LAI/FPAR retrievals within each tile, which are subsequently aggregated to 8-day composites based on the selection of the maximum FPAR value and the corresponding LAI for each pixel (Yang et al., 2006a). We compared the retrieval characteristics of both the collection 4 (C4) and collection 5 (C5) products. The C4 product has been validated across a variety of vegetation types (e.g. Cohen et al., 2006; Fensholt et al., 2004; Garrigues et al., 2008), including boreal forests (Abuelgasim et al., 2006; Pisek & Chen, 2007; Steinberg et al., 2006). The C5 product has undergone only minimal validation (e.g. De Kauwe et al., 2011; Fang et al., 2012; Sea et al., 2011; Shabanov et al., 2005). In addition, we assessed the intermediate FPAR product (C4.1), which was developed

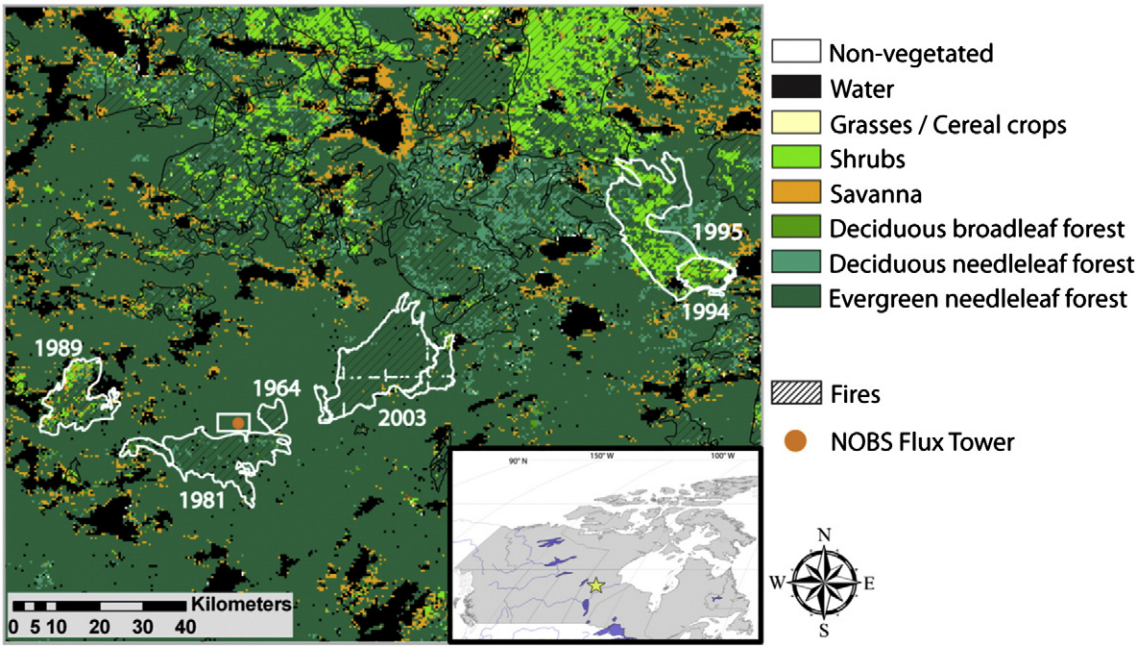

Fig. 1. The location of the seven study sites comprising the wildfire chronosequence overlaid on the 2006 MODIS MCD12Q1 C5 landcover product. The burn perimeters for the 1981 to 2003 burns are derived from the Canada Large Fire Database (CLFDB, Stocks et al., 2003), while the 1964 burn perimeter was delineated by hand using historic imagery. The boundary for the oldest, 1930 and 1850 burn sites is shown by the white rectangle. The location of the Northern Old Black Spruce site flux tower (NOBS, Sellers et al., 1997b) at the heart of the 1850 burn is shown as the filled orange circle. Inset map shows the location of the study sites in north-central Manitoba, Canada.

to circumvent a coding error that was found in the original C4 FPAR data. Unless otherwise stated, all FPAR analyses and figures comparing the two MODIS collections pertain to the C4.1 FPAR dataset. We included the C4 FPAR data (see Fig. 9, Results and Discussion sections), however, because several previous validation studies (e.g. Fensholt et al., 2004; Steinberg et al., 2006) utilized the earlier C4 FPAR product.

The main biophysical retrieval algorithm for both the C4 and C5 versions is based on the look-up table (LUT) values that are derived from one- to three-dimensional radiative transfer model (RTM) simulations over biome-specific vegetation types (Knyazikhin et al., 1998; Shabanov et al., 2005). The significant changes between the two versions are an expanded biome classification from six (C4) to eight biomes (C5) and an improved set of LUTs optimized for broadleaf forests (Shabanov et al., 2005; Yang et al., 2006b). Inputs of the RTM include atmospherically corrected surface reflectance from the MODIS red and near-infrared bands (Vermote et al., 1997) and scene sun-sensor geometry. The RTM outputs are the mean LAI and FPAR computed over the acceptable range for which simulated and observed MODIS surface reflectance values differ within specified uncertainty levels (Knyazikhin et al., 1998; Shabanov et al., 2005). The updated C5 product now includes the standard deviation (i.e. uncertainty) of the estimated values for each pixel (Shabanov et al., 2005). A lower accuracy backup algorithm based on LAI/FPAR–NDVI relationships derived from the RTM simulations is used when the main algorithm fails, such as in the cases of reflectance saturation, residual atmospheric contamination, or snow cover (Yang et al., 2006a). Vegetation clumping at the shoot and canopy scales was accounted for in the RTM formulation and at the landscape scale by utilizing canopy spectral invariants (Huang et al., 2007; Knyazikhin et al., 1998).

2.3. LAI and FPAR ground measurements

We measured the effective LAI (L_e) and fraction of photosynthetically active radiation (FPAR) absorbed by the vegetation at ground-level

Table 1
Biophysical characteristics of the seven wildfire chronosequence sites used in this study. The LAI and FPAR of the overstory and total canopy were measured indirectly using optical instruments (see Methods section). The values in parentheses represent the ±one standard deviation of the mean.

Site characteristics	Year of burn (age [a])						
	2003 (1)	1994/95 (10/11)	1989 (15)	1981 (23)	1964 (40)	1930 (74)	1850 (154)
Latitude °N	55.94	56.17	55.91	55.86	55.92	55.91	55.88
Longitude °W	−98.08	−96.73	−98.97	−98.48	−98.40	−98.52	−98.50
Mean tree diameter (cm)	–	4.04	4.74	8.40	8.80	9.42	10.1
Basal area (m^2 ha^{-1})	–	1.60	1.94	25.7	13.8	25.4	31.3
Canopy LAI (m^2 m^{-2})[b]	0.1 (0.38)	0.33 (0.58)	0.85 (1.11)	2.03 (1.37)	1.82 (0.92)	3.74 (1.22)	3.64 (0.80)
Total LAI (m^2 m^{-2})[c]	0.68 (0.57)	1.30 (0.75)	1.90 (1.16)	3.19 (1.60)	2.82 (1.17)	4.30 (1.75)	4.10 (1.18)
Canopy FPAR	0.15 (0.16)	0.24 (0.22)	0.44 (0.29)	0.67 (0.28)	0.56 (0.23)	0.70 (0.25)	0.73 (0.16)
Total FPAR	0.30 (0.18)	0.58 (0.18)	0.72 (0.18)	0.84 (0.16)	0.77 (0.14)	0.81 (0.14)	0.80 (0.13)
Elevation range (m)	200–288	179–222	243–322	240–303	241–280	250–278	237–291

Elevation data are derived from SRTM digital elevation data (http://landval.gsfc.nasa.gov/).
[a] Forest age in 2004.
[b] Canopy LAI refers to the LAI measurement greater than 1 m above the ground (see Fig. 2).
[c] Total LAI refers to the LAI measurements made at ground level (see Fig. 2).

(LAI_T and $FPAR_T$) and above the understory vegetation (LAI_O and $FPAR_O$), at a height of about 1 m (Fig. 2), using the LAI-2000 Plant Canopy Analyzer (Li-Cor Inc., Lincoln, NE). Understory LAI (LAI_U) was calculated as the difference between the total LAI (LAI_T) and overstory (LAI_O). The LAI_O was calculated using Eqs. (1) and (2) for the coniferous (LAI_C) and deciduous (LAI_D) forests, respectively:

$$LAI_c = \frac{(1-\alpha)L_e\gamma_E}{\Omega_E} \quad (1)$$

$$LAI_D = \frac{L_e}{\Omega} - \alpha \quad (2)$$

where L_e is the effective LAI, γ_E is the needle-to-shoot area ratio, Ω_E is the elemental clumping index, α is the woody-to-total leaf area ratio ($\alpha = W/L_e(\gamma_e/\Omega_E)$), and W represents the woody-surface-area-index (half the woody area m^{-2} ground area). We used values of γ_E, α, Ω_E for boreal tree species derived from the literature (Chen & Cihlar, 1995; Chen et al., 1997; Gower et al., 1999) and estimated α using average leaf-off LAI-2000 measurements (Serbin et al., 2009).

We calculated in situ FPAR for the overstory ($FPAR_O$) and total ($FPAR_T$) vegetation strata from the LAI-2000 measurements by subtracting the canopy transmittance values at each measurement height (Fig. 2) from unity as:

$$FPAR = 1 - \tau \quad (3)$$

where τ is the fraction of light transmitted through the canopy determined from the optical measurements (i.e. τ = diffuse non-interceptance, DIFN or integrated gap fraction). $FPAR_U$ was then calculated as the difference between $FPAR_T$ and $FPAR_O$. Given that our measurements include the interception of radiation by foliage and non-photosynthetic material (e.g. branches) and that we don't account for PAR reflected back from the canopy by foliage or the ground (which is generally minimal), we define our in situ FPAR as: FPAR≈FIPAR (1-intercepted PAR/incident PAR). However, FIPAR generally approximates FPAR in most conditions (Gobron et al., 2006; Gower et al., 1999; Huemmrich et al., 2005).

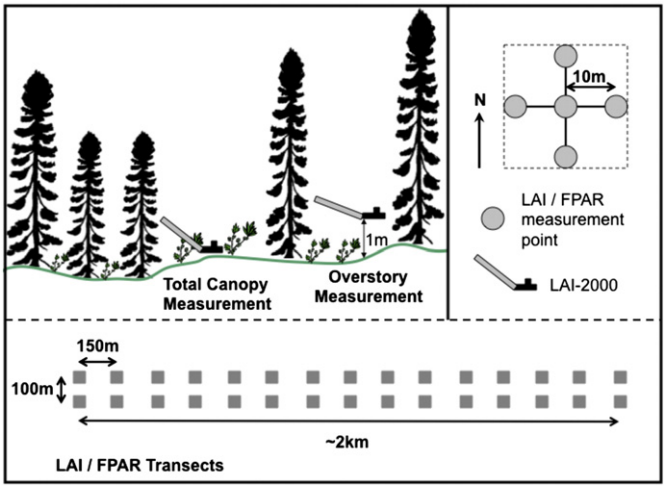

Fig. 2. Design of the LAI-2000 field sampling protocol for measuring overstory and total LAI and FPAR across the two kilometer total transects within the seven study sites (Fig. 1). The total canopy LzAI and FPAR (LAI_T and $FPAR_T$) were measured with the LAI-2000 sensor head held near the ground layer, below the understory herbaceous and shrub layer, while the overstory LAI and FPAR (LAI_O and $FPAR_O$) were measured above the understory layer at a height of about 1 m. Note that the contribution of low-stature ground-cover vegetation, including bryophytes, was not included in the measurements, but can represent a large fraction total stand LAI in boreal forests (Bond-Lamberty & Gower, 2007). The inset shows the five subplot locations where LAI and FPAR were measured for the over- and understory strata at each sample plot.

We measured the LAI and FPAR at thirty plots along a pair of 2 km transects within each burn site (Fig. 2). The transects were separated by 100 m and each plot was separated by 150 m along each transect. At each plot we established five subplots, one at plot center and four other subplots at 10 m from plot center in the four cardinal directions (Fig. 2). Each plot mean for the overstory vegetation and understory vegetation was calculated from five individual LAI-2000 measurements taken at each subplot, one measurement above and one below the understory. A reference LAI-2000 was located on the top of a nearby scaffold tower (approximately 5 m above the canopy) and programmed to collect data every 15 s. A 270° view cap was used on the reference and all measurement LAI-2000s to mask the operator from the field of view of the sensor. Reference and field measurements were taken simultaneously and were collected in the early morning, at dusk, or during periods of uniform diffuse sky radiation (Serbin et al., 2009).

The LAI-2000 sample dates spanned the range of growing season phenology from pre-leaf emergence (i.e. leaf-off) through the onset of canopy senescence (Serbin et al., 2009). We adopted the following terminology based on visual observations; (i) leaf-off: no foliage on deciduous trees, buds may be present and no green understory; greenup: period of canopy development by deciduous species, understory vegetation was leafing-out; canopy maturity: canopy and understory canopy complete or quasi-stable; onset of canopy senescence: beginning of leaf coloring and reduction in understory biomass.

2.4. Automated measurements of FPAR

To obtain a continuous record of incident and intercepted photosynthetically active radiation (PAR), automated measurements were made using LI-191SA Line Quantum Sensors (Li-Cor BioSciences, Lincoln, NE). At each site, up to four line quantum sensors were positioned in the four cardinal directions below the canopy at maximum cable length (32 m). An additional sensor was mounted on a tower above the canopy to capture incident PAR. The below canopy LI-191SA sensors were installed on two metal stakes to ensure they were level and above the ground surface to avoid damage from surface moisture. The sensors were deployed in each site in early spring (~DOY 110) to capture the seasonal dynamics of canopy light interception by vegetation (i.e. FPAR) and maintained throughout the growing season. The sensors were removed in October (~DOY 295). The first growing season (2004) had fewer measurements because we were establishing instruments at all the sites. Further details of the collection and post-processing of these data can be found in Serbin et al. (2009).

2.5. Development of LAI and FPAR reference maps

A key issue in the evaluation of moderate resolution data products, such as the MODIS MOD15A2 LAI/FPAR product, is the spatial disparity between ground-based measurements and retrieved values. A common approach consists of using high spatial resolution imagery (15–30 m) as an intermediary to scale plot-based LAI and FPAR measurements up to the grain size of the moderate resolution pixel (Morisette et al., 2006).

For this study we utilized the Advanced Space-borne Thermal Emission Reflection Radiometer (ASTER, Abrams et al., 2002) level-2 atmospheric and cross-talk corrected surface reflectance data products (AST07XT). The 15 m and 30 m nominal resolution in the VNIR and SWIR spectral regions, respectively, of ASTER were used to derive fine scale biophysical maps based on field measurements of LAI and FPAR to evaluate MODIS data. We selected scenes that coincided with maximum growing-season LAI, were close to the sample dates,

Table 2
The MODIS MOD12Q1 (C4) and MCD12Q1 (C5) landcover statistics for the seven study sites comprising the wildfire chronosequence. The observed percent black spruce is provided for comparison with the MODIS landcover estimates of needleleaf cover across the chronosequence as this species was the dominant needleleaf tree observed in our sites (when present). The estimates of black spruce cover are derived from the observations of tree basal area measured within each burn site. Note the 2003 burn scar may not have been present during the generation of the MODIS C4 landcover product (Friedl et al., 2002, 2010).

	Cover class percentage (%) for burn sites					
	Age since fire:					
Type 3 classes	1 (2003)	10/11 (1994/95)	15 (1989)	23 (1981)	40 (1964)	74 (1930)/154 (1850)
	C4/C5	C4/C5	C4/C5	C4/C5	C4/C5	C4/C5
Water	2.1/0.6	5.3/3.7	8.4/6.5	0.0/6.5	0.0/1.6	0.0
Grasses/cereal crops	0.4/0.0	41.3/1.7	0.6/0.6	0.8/0.6	0.0	0.0
Shrubs	0.9/0.5	25.3/42.3	11.2/11.2	0.4/11.2	0.0	0.0
Broadleaf crops	0.0/0.0	0.0/0.0	0.0/0.0	0.0/0.0	0.0	0.0
Savanna	0.7/0.6	0.0/5.0	14.6/12.6	7.6/12.6	0.0	0.0
Broadleaf forest	0.0/0.0	0.0/0.0	0.0/1.4	0.8/1.4	0.0	0.0
Needleleaf forest	95.3/98.0	28.0/41.3	65.2/57.3	90.3/57.3	100.0/96.1	100.0/100.0
Deciduous needleleaf	n.a./0.5	n.a./6.0	n.a./10.4	n.a./10.4	n.a./2.4	n.a./0.0
Unvegetated	0.2/0.0	0.0/0.0	0.0/0.1	0.0/0.1	0.0	0.0
Total percent	100.0	100.0	100.0	100.0	100.0	100.0
Observed % black spruce	0.0	0.5	2.0	9.0	46.0	90-97

and were relatively cloud free. The ASTER data were obtained from the BOREAS NSA EOS land validation core site.[2] An orthorectified Landsat-7 Earthsat ETM + scene, acquired on September 9th, 2001 was used as the reference image to improve the locational accuracy of each ASTER scene.

We used an empirical regression modeling approach to derive the transfer functions to relate the field measurements to the ASTER data (Cohen et al., 2003; Steinberg et al., 2006; Tan et al., 2005; Wang et al., 2004). For this we used a partial least-squares regression (PLSR, Geladi & Kowalski, 1986; Wold et al., 1984; Wolter et al., 2008) approach to generate the models used to map LAI and FPAR with ASTER surface reflectance and spectral vegetation indices (SVI's). The PLSR method relies on the optimization of the covariance structure between predictor and response variables to develop a series of component factors which capture the predictor variance and are highly correlated with the response variables (Geladi & Kowalski, 1986; Wold et al., 1984; Wolter et al., 2008). The benefits of PLSR are that it does not assume the predictor data are measured without error, which is often falsely assumed for image data (Huang et al., 2006) and avoids the issues of collinearity between predictor variables by generating the coefficients from the decomposition of the predictor variables. PLSR has been used previously to calibrate models for mapping biochemical and biophysical parameters using remotely sensed data (e.g. Smith et al., 2002; Townsend et al., 2003) and forest composition and structure using multi-spectral data (e.g. Wolter et al., 2008).

We used a custom iterative variable selection method (Serbin et al., 2012; Wolter et al., 2008) in combination with the PLS-REGRESS routine in Matlab (Mathworks, Natick, MA) to derive the set of most informative predictors from the full set of variables. This approach produces the most parsimonious models and avoids over fitting issues associated with high numbers of component factors and predictor redundancy (Wolter et al., 2008). The starting set of predictors included the nine ASTER surface reflectance bands and several commonly used SVIs for LAI-FPAR mapping (e.g. NDVI, SR, SAVI, NDWI, MSI), as well as the short-wave visible (SVR) ratio (Wolter et al., 2008). Each PLSR model was validated using a leave-one-out cross validation.

The resulting ASTER-based LAI and FPAR maps were then aggregated to MODIS resolution (i.e. 1-km) by averaging only the ASTER pixels completely filling each MODIS pixel within a 7×7 km area (Cohen et al., 2006) centered on the sample transects. This was done within each burn site and resulted in a maximum potential number of pixels for comparison equaling 49 per site.

3. Results

3.1. Reflectance characteristics across burn sites

The average peak growing season MODIS MOD09 NDVI values ranged from (±one standard deviation) a minimum of 0.69 (±0.06) in the 2003 burn to a maximum of 0.81 (±0.05) in the 1930 and 1850 burns. The dormant season snow-free NDVI values (i.e. seasonal minimums) increased with time since fire and relative canopy dominance by black spruce (Table 2), ranging from a minimum of 0.45 for the early successional sites (1989–2003 burns) to a maximum of 0.61 for the older conifer forests (1930 and 1850 burns).

Prior to fire, the 2003 burn displayed a seasonal pattern similar to the oldest sites (not shown) with an annual maximum NDVI near 0.8 and elevated NIR and red reflectance values, which were higher in the NIR than the red in the winter due to the complex mix of conifer trees and a snow-covered background (Fig. 3). Immediately following fire, the wintertime reflectance increased sharply, summertime NDVI decreased, and the seasonal minimum NDVI approached zero. The rapid rise in winter red and NIR reflectance is likely associated with the loss of evergreen foliage and increased visible snow cover in winter. Presumably, the standing charred black spruce snags, as well as the burned and exposed mineral soil, also contributed to the changes in MODIS reflectance, along with patches of unburned mosses, primarily *Shagnum* spp. in lowlands, and small pockets of live black spruce trees which survived the fire (Fig. 3). Peak summertime NDVI rapidly increased in subsequent years and reached values similar to the 1994 and 1989 burns within two years, likely due to the observed recovery of a vigorous herbaceous layer and the establishment of evergreen species such as black spruce seedlings and labrador tea (Fig. 3).

MODIS NDVI was strongly correlated with in situ LAI_U ($r = 0.73$), LAI_O ($r = 0.62$), and the total LAI (LAT_T, $r = 0.59$) for the sites comprising the wildfire chronosequence. NDVI had the highest correlation with the seasonality of the understory vegetation (LAI_U $r = 0.81$ versus LAI_O $r = 0.56$) for the youngest sites (1994 and 2003 burns), but also displayed a generally strong relationship with the seasonality of LAI_U ($r = 0.83$) across the five early- to mid-successional sites (2003–1964 burns). In addition, MODIS NDVI displayed a strong correlation ($r = 0.68$) with the seasonal variation in overstory vegetation (LAI_O) for the mid-successional sites (1989–1964). These sites generally contained a significant proportion of deciduous tree species (e.g. aspen). For the

[2] http://landval.gsfc.nasa.gov/.

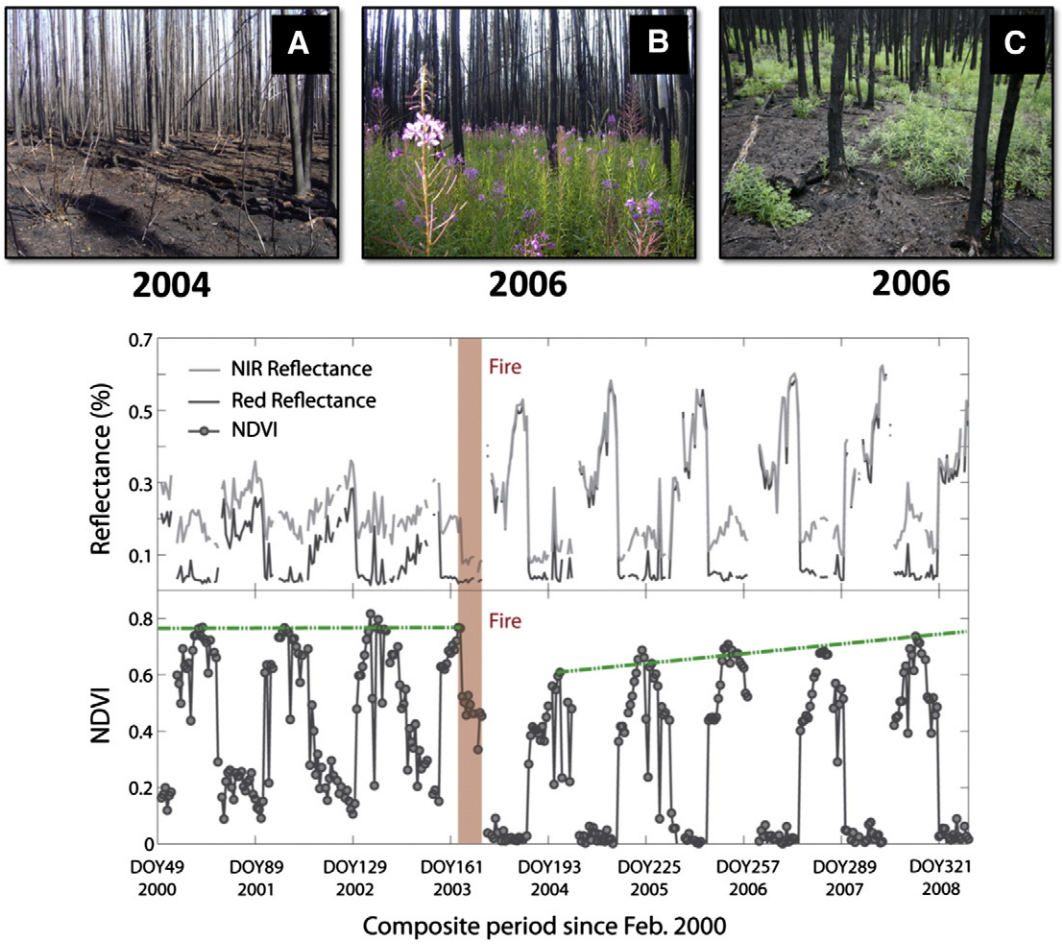

Fig. 3. Post-fire photographs from the 2003 wildfire study site one year following fire (A) and two years post-fire (B & C) illustrating the degree of fire severity and the patchiness of the herbaceous layer recovery. Pre- and post-fire MODIS MOD09 red reflectance, NIR reflectance, and NDVI seasonal trajectories, with the pre-fire and post-fire NDVI trends superimposed (green line) to highlight the quasi-stable maximum pre-fire values as well as the rapid recovery in NDVI following the fire. (For interpretation of the references to color in this figure legend, the reader is referred to the web version of this article.).

oldest sites (1930 and 1850 burns) MODIS NDVI displayed the highest correlation with understory vegetation (LAI_U $r = 0.46$) and displayed a poor correlation ($r = 0.06$) with the overstory LAI (LAI_O), which was comprised primarily of black spruce trees (Table 2).

3.2. Direct validation of the MODIS LAI and FPAR products

The quality of collection 4 (C4) and collection 5 (C5) MODIS LAI and FPAR products were poorest during winter, the early spring, and late fall, while the best quality retrievals occurred in mid-growing season (Fig. 4). This coincided with the longest contiguous snow-free period and the interval of best sun-sensor geometry. On average, we observed a 72% increase in main RT retrievals following DOY 105 for both C4 and C5 products. During the winter months, the values were largely derived from backup algorithm retrievals due a lower solar angle resulting in elongated shadowing and high snow cover. Throughout the entire study period (2004–2006), the C5 product had a 30% higher rate of main RT LAI and FPAR solutions compared to the C4 product, while QC2 retrievals (i.e. back-up algorithm used because of bad geometry) remained relatively constant between the two products for ~DOY 300–DOY50 period (i.e. fall through late winter).

The MODIS MOD12Q1 (collection 4) landcover type 3 classification used in the MOD15A2 algorithm classified the majority of the landscape as needle-leaf evergreen forests, except the 1994 burn site, which was classified as 41% grasses and cereal crops, 25% shrubs, and a minor component classified as water (Table 2). The best agreement between observed vegetation cover and the MODIS landcover product occurred in the two oldest forests (1930 and 1850), where black spruce dominated the overstory canopy, and the largest disparity occurred in the early-successional to mid-successional sites (2003–1964 burns). The updated C5 landcover product (MCD12Q1) classified the majority of the landscape as needleleaf evergreen forest (Fig. 1); however, the C5 scheme included the new deciduous needleleaf forest class. This class comprised only a small fraction of our sites (Table 2), however it was present across the larger landscape (Fig. 1). We also observed that the percent needleleaf forest cover increased and decreased slightly for the 10-year-old and 15-year-old sites, respectively, in the updated C5 landcover product (Table 2).

The in situ total and overstory FPAR ($FPAR_T$ and $FPAR_O$) exhibited significant variation along the chronosequence, displaying a minimum in the youngest, early successional burn sites and maximum in the oldest, needle-leaf evergreen dominated forests (Table 1). Collectively, the MODIS C5 retrievals were well correlated with seasonal in situ LAI-2000 $FPAR_T$ measured along transects ($y = 0.56x + 0.26$, $r^2 = 0.71$) but tended to overestimate and underestimate FPAR in the early successional and late successional sites, respectively (Fig. 5). Compared to the C5 data, the previous collection 4.1 FPAR data displayed a weaker relationship and a higher overall offset from the LAI-2000 $FPAR_T$ ($y = 0.11x + 0.68$, $r^2 = 0.26$); the original C4 FPAR offset was 13% higher than C4.1 at 0.78. For both the MODIS C4.1 and C5 data, the disparity between MODIS and in situ FPAR generally decreased with increasing FPAR (i.e. time since fire and increasing needle-leaf cover, Fig. 5) and was less for $FPAR_T$ than $FPAR_O$ (not shown).

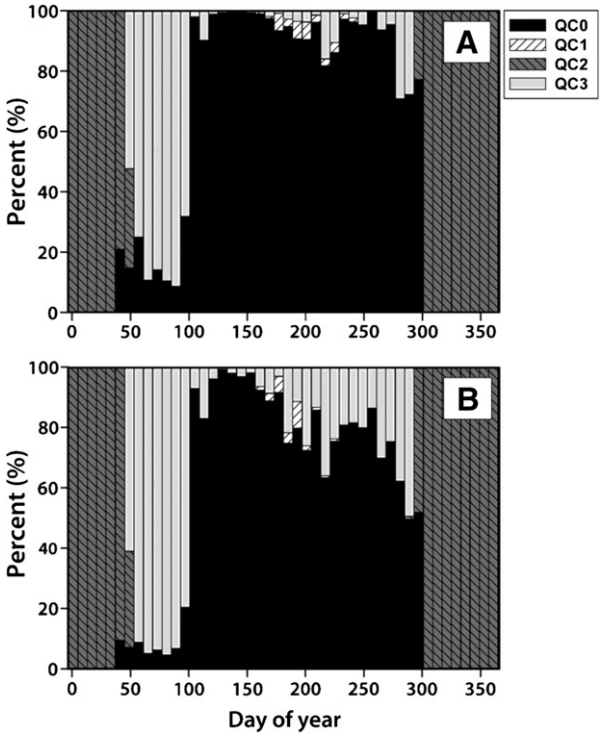

Fig. 4. Average (2004 through 2006) annual course in the MODIS collection 5 (A) and collection 4 (B) LAI/FPAR QC statistics across the seven study sites, shown by compositing period: the percentage of main algorithm retrievals (QC0, black), the percentage of main algorithm retrievals under conditions of saturation (QC1, hatched white), the percentage of backup (i.e. NDVI-based) retrievals associated with bad geometry (QC2, hatched dark gray), and the percentage of pixels using the backup algorithm due to reasons other than geometry (QC3, light gray). Note the overall increase in high quality (QC0) retrievals from the C4 (B) to C5 (A) data during the middle of the growing season.

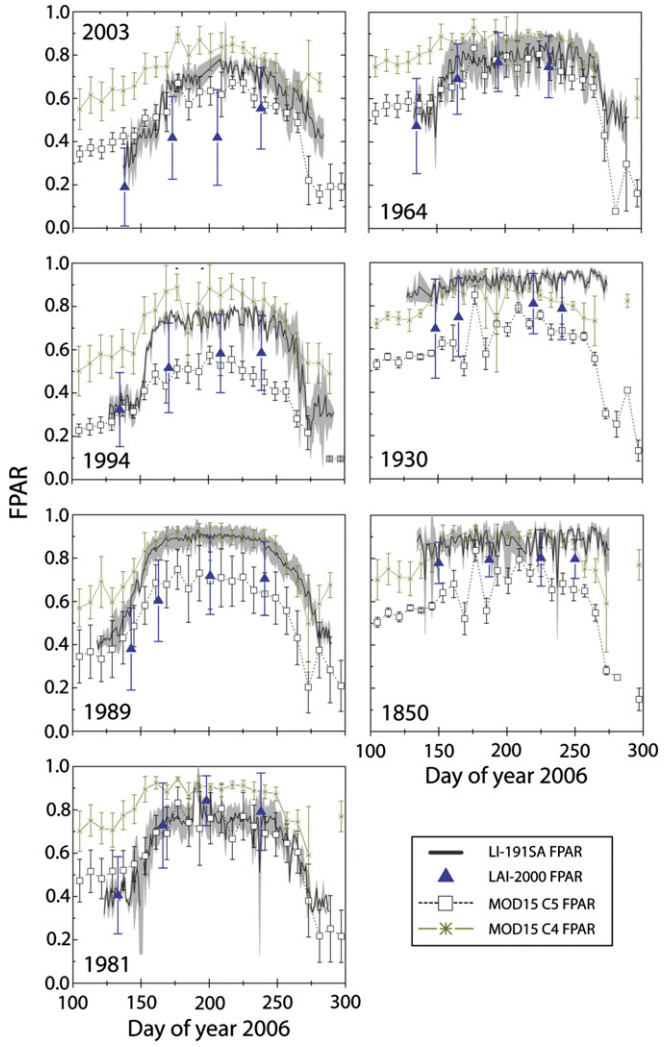

Fig. 5. Comparisons between the MODIS C4 and C5 FPAR seasonal trajectories and in situ FPAR along the wildfire chronosequence, during the 2006 growing season. The gray shaded area represents the ±one standard deviation of the mean LI-191SA daily FPAR values, while the vertical bars represent the ±one standard deviation of the mean LAI-2000 or MODIS FPAR values for each period. Note that the LAI-2000 values represent the transect means (±one standard deviation) for each measurement period.

The FPAR phenology varied significantly across the sites due to differences in vegetation density, composition, and age with the youngest, deciduous dominated forests showing a greater seasonality compared to the oldest, conifer dominated sites (Fig. 5). MODIS FPAR generally tracked the seasonal progression of in situ LI-191SA FPAR including the important greenup, peak foliar biomass, and senescent periods of the vegetation. The seasonal correlation was highest in the early- to mid-successional sites that typically displayed the largest seasonality in FPAR, while in the oldest, 1930 and 1850 burn sites, MODIS FPAR was not correlated with in situ values (Table 3). For these sites, MODIS generally displayed greater variation in retrieved values than in situ FPAR during the growing season (Fig. 5). Overall, the MODIS C5 FPAR data displayed a higher agreement with growing season FPAR derived from the LI-191SA sensors than the previous C4 data (Table 3). This may be related to the increased use of main RT algorithm retrievals during the growing season in the C5 compared to the C4 MODIS data (Fig. 4).

As with FPAR, the in situ LAI increased significantly with forest age and showed greater variability in the mid- to late-successional sites (Table 1). The 2005 and 2006 observed LAI_T displayed a typical seasonal pattern across the chronosequence, with the youngest, deciduous dominated burns showing a greater seasonality than the later successional, evergreen conifer dominated sites (Fig. 6). Similarly, MODIS LAI seasonal time series showed comparable LAI phenology for both the C4 and C5 versions, with LAI increasing in the spring to a relatively stable maximum in mid-July (~DOY 193), and decreasing at the end of the growing season to a quasi-stable background value. The C5 LAI product showed a stronger seasonal correlation with in situ LAI_T ($y = 0.29x + 1.17$ $r^2 = 0.24$) than the previous C4 LAI data ($y = 0.29x + 3.14$, $r^2 = 0.15$). Both the C4 and C5 versions displayed a much greater seasonality in LAI for the oldest, 1930 and 1850 burn sites compared to the in situ LAI_T (Fig. 6). Excluding these sites significantly improved the relationship between C5 and in situ LAI ($y = 0.74x + 0.60$, $r^2 = 0.59$). Across the chronosequence, there was a clear break between the DOY 97 and DOY 105 compositing period

Table 3
Pearson correlation coefficients of the seasonal comparison between MODIS MOD15A2 and 8-day averaged LI-191SA in situ timeseries FPAR observations across the wildfire chronosequence. The differences in sample size are due to the timing of in situ sensor deployment (see Methods section) and various instrument failures during the growing seasons. The sample sizes were intentionally kept consistent between the C4.1 and C5 MODIS products.

Burn Site	Sample Size	Correlation (r)	
		C4.1 (*p*-value)	C5 (*p*-value)
2003	30	0.58 (0.002)	0.69 (0.002)
1994	42	0.75 (<0.001)	0.77 (<0.001)
1989	60	0.81 (<0.001)	0.84 (<0.001)
1981	40	0.75 (<0.001)	0.86 (<0.001)
1964	51	0.57 (<0.001)	0.74 (<0.001)
1930	47	−0.12 (0.51)	0.17 (0.16)
1850	31	−0.06 (0.70)	0.02 (0.46)
All sites	296	0.58 (<0.001)	0.60 (<0.001)

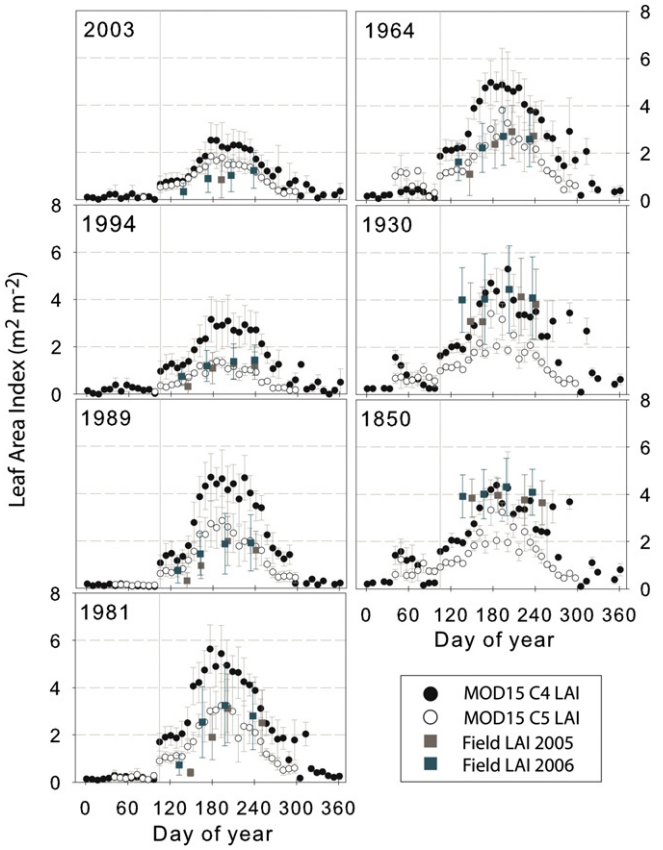

Fig. 6. The seasonal pattern of MODIS C4 and C5 LAI compared to observed values for years 2005 and 2006. Note the MODIS data are averaged by year and compositing period. The error bars represent the ±one standard deviation of the mean MODIS or in situ LAI observation during the composite period. The vertical gray bar shows the location where there is a consistent and rapid increase in MODIS LAI (~DOY105) that is related to the rapid increase in high-quality LAI retrievals (Fig. 4).

for the C4 and C5 data (Fig. 6, vertical line), which corresponds to a rapid increase in high-quality LAI retrievals (Fig. 4). These high-quality retrievals (QC0) continue until the DOY 305 compositing period when we observed a rapid increased use of backup algorithm retrievals, which continued through the winter months (Fig. 4).

3.3. MODIS validation with high-resolution LAI and FPAR maps

We observed strong positive correlations between field measurements and predicted (derived from the PLSR cross-validation procedure) values of LAI and FPAR based on ASTER reflectance and SVIs (Fig. 7). In all cases the bias was zero and the variance ratio was minimal, indicating no bias in the predications and only small compression in the variance of the predicted values for each variable (Fig. 7). In addition, the uncertainty of prediction (i.e. RMSE) was lower for the total LAI and FPAR compared to the overstory transfer functions, suggesting increased error associated with mapping only overstory leaf area in these relatively open canopy forests.

The MODIS C4 data substantially overestimated the ASTER reference LAI_T for the young- to mid-successional (i.e. 2003–1964) burn sites (Fig. 8), with a mean difference (MD, ±one standard deviation) between MODIS and ASTER-based values of 1.54 (± 1.45 m^2 m^{-2}) and a mean absolute difference (MAD) of 1.85 (± 1.03 m^2 m^{-2}). We observed a better correlation between the ASTER LAI_T reference maps and MODIS C4 data for the oldest, evergreen needleleaf sites (i.e. 1930 and 1850), with a MD of −0.34 (± 0.94 m^2 m^{-2}), while the poorest agreements were observed over the 1980's burn sites (1989 and 1981) with a MD of 2.69 (± 0.83 m^2 m^{-2}).

The LAI estimates were substantially better for the C5 product, with an overall reduction in RMSE and MD between MODIS and ASTER LAI_T reference maps of 61% and 69%, respectively (Table 4, Fig. 8). The large discrepancies in the deciduous and mixed deciduous/evergreen sites (i.e. 2003–1964) were greatly reduced in C5 data (Table 4), with a MD of 0.54 (± 63 m^2 m^{-2}). However, the C5 data still underestimated the maximum LAI for needleleaf sites by an average of 14% (Figs. 6 & 8, Table 4). In both cases (i.e. C4 versus C5), a lower

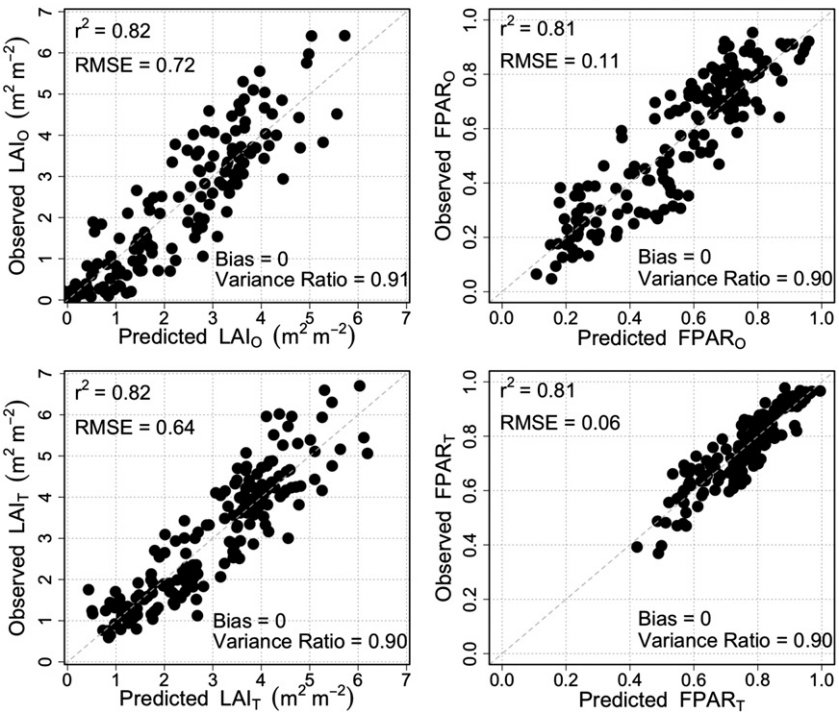

Fig. 7. Observed versus predicted PLS transfer functions between ASTER spectral vegetation indices (SVIs) and in situ overstory and total LAI and FPAR. The bias and variance ratio are defined in Cohen et al. (2006).

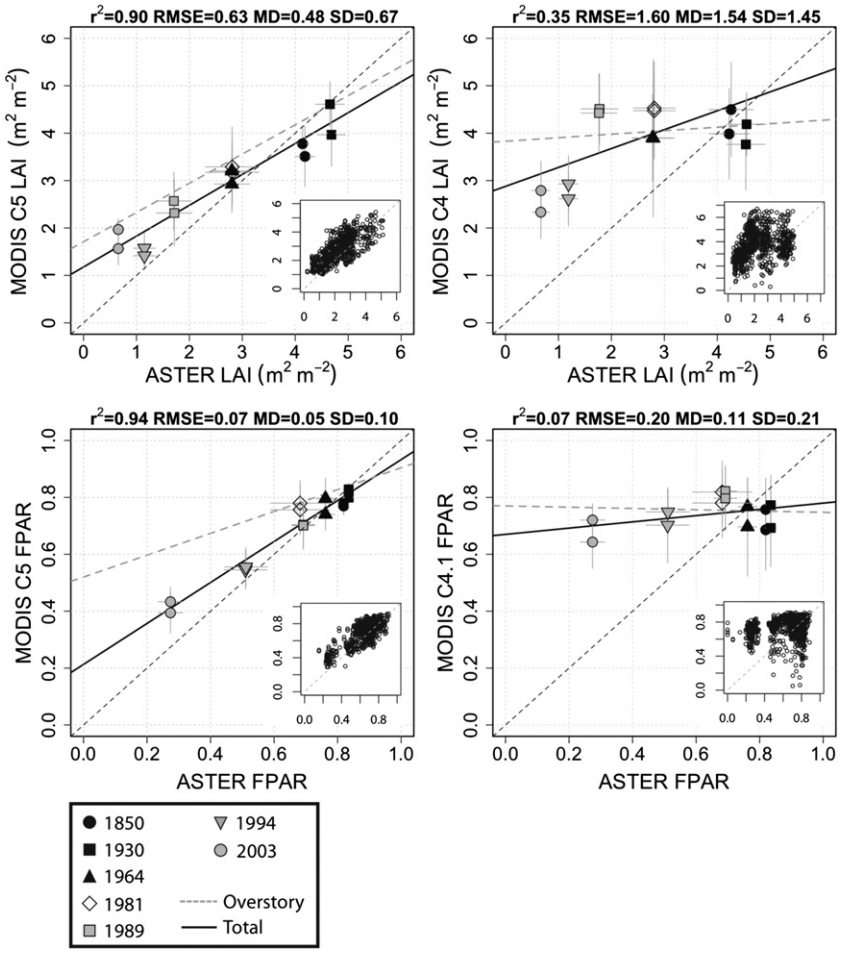

Fig. 8. Spatial validation of the MODIS C4 and C5 LAI and FPAR products using the high-resolution ASTER-derived biophysical maps, aggregated to MODIS resolution (i.e. 1 km). The solid black regression lines and statistics pertain to the relationship between the ASTER-based LAI_T and $FPAR_T$ maps and MODIS retrievals, while the dashed gray lines show the relationship between MODIS and the reference LAI_O and $FPAR_O$ values. The inset figures show the pixel-by-pixel comparison between ASTER reference maps and MODIS across the chronosequence. The horizontal and vertical error bars represent the ±one standard deviation of the mean LAI or FPAR value for ASTER and MODIS, respectively, within the 7×7 km subset region per burn site.

overall bias was observed between MODIS retrievals and the ASTER reference maps based on total canopy LAI versus overstory LAI alone (Table 4, Fig. 8).

The ASTER $FPAR_T$ reference maps displayed a large range in values across the chronosequence (Figs. 8 & 9) and were similar to in situ values (Table 1). In contrast, the MODIS C4.1 FPAR product displayed a much smaller dynamic range in retrieved values and larger within-site variability. The weakest relationship between the reference maps and MODIS C4.1 was for the youngest 2003 burn, with a MD of 0.43 (±0.1) and an overall bias between MODIS and ASTER $FPAR_T$ reference maps of 0.67 (Fig. 8). In contrast, the overall difference between reference values and MODIS FPAR was 55% lower in the C5 than previous C4.1 FPAR product (Fig. 8, Table 4) and retrieval variability dropped by 52%. The largest difference between ASTER $FPAR_T$ and C5 MODIS

Table 4
Summary of the mean difference (±one standard deviation) between MODIS retrievals and the ASTER-based LAI and FPAR maps (derived from in situ measurements) within the 7×7 km subsets. The 2003 burn site did not have a significant overstory at the time of sampling (i.e. 2004–2006). Note that a positive value indicates a general overestimation by MODIS while a negative value indicates an underestimation of MODIS LAI or FPAR.

Burn Site	Canopy	LAI (m^2 m^{-2})		FPAR (−)	
		C4	C5	C4	C5
2003	Overstory	–	–	–	–
	Total	1.88 (±0.62)	1.11 (±0.32)	0.43 (±0.10)	0.14 (±0.06)
1994	Overstory	2.20 (±0.57)	0.99 (±0.23)	0.56 (±0.14)	0.40 (±0.06)
	Total	1.58 (±0.58)	0.34 (±0.28)	0.20 (±0.12)	0.04 (±0.07)
1989	Overstory	3.64 (±0.78)	1.53 (±0.63)	0.43 (±0.09)	0.33 (±0.08)
	Total	2.70 (±0.70)	0.73 (±0.61)	0.12 (±0.08)	0.01 (±0.07)
1981	Overstory	3.88 (±0.93)	1.41 (±0.72)	0.16 (±0.14)	0.13 (±0.10)
	Total	2.68 (±0.92)	0.41 (±0.72)	0.09 (±0.15)	0.09 (±0.11)
1964	Overstory	2.11 (±1.29)	1.27 (±0.54)	0.07 (±0.16)	0.12 (±0.07)
	Total	1.11 (±1.29)	0.26 (±0.53)	−0.04 (±0.15)	0.01 (±0.06)
1930	Overstory	−0.04 (±0.90)	0.14 (±0.67)	0.00 (±0.13)	0.05 (±0.04)
	Total	−0.61 (±0.89)	−0.41 (±0.66)	−0.08 (±0.13)	−0.02 (±0.04)
1850	Overstory	0.30 (±0.99)	−0.04 (±0.46)	0.01 (±0.13)	0.05 (±0.04)
	Total	−0.05 (±0.91)	−0.52 (±0.47)	−0.09 (±0.13)	−0.05 (±0.03)

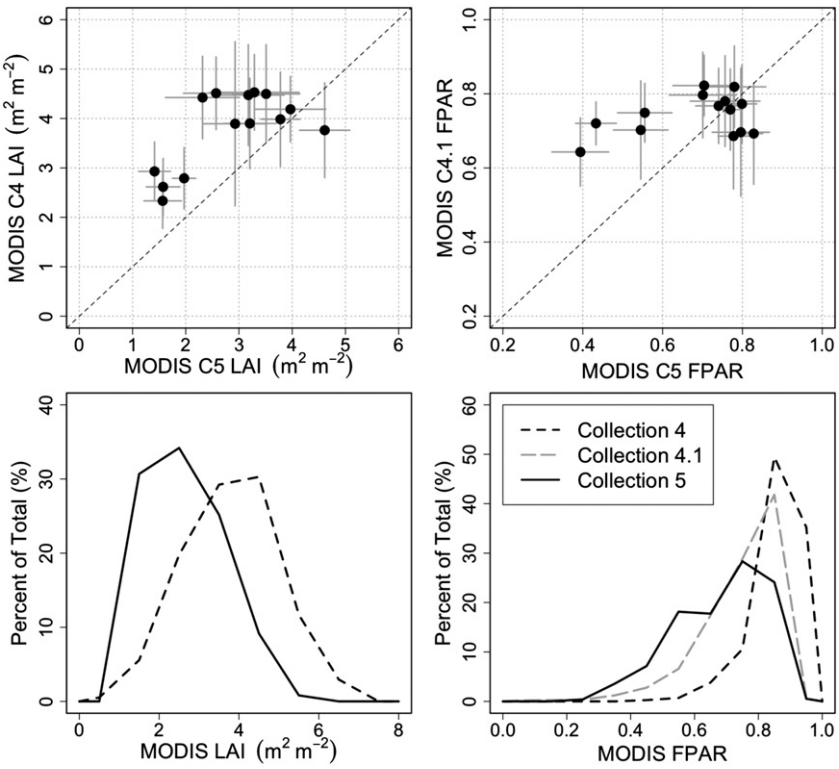

Fig. 9. Comparison between the 2005 & 2006 MODIS C4 and C5 LAI and FPAR algorithm retrievals, averaged across the seven study sites (top left and right). The error bars represent the ±one standard deviation of the mean retrieval value across each burn site and version of the MODIS LAI/FPAR product. The distribution of retrievals across the entire study region (bottom left and right) shown for the C4, intermediate C4.1 and current C5 LAI and FPAR products.

data remained in the 2003 burn site, but the difference decreased to 0.14 (±0.06), and the overall bias (i.e. regression intercept) declined to 0.18 (Fig. 8). Similar to LAI, the correspondence between the MODIS C5 FPAR and ASTER-based maps was higher for $FPAR_T$ than $FPAR_O$ reference maps (Table 4, Fig. 8).

3.4. Comparison between the MODIS C4 and C5 products

The C4 and C5 MODIS LAI and FPAR products generally displayed similar seasonal patterns across the chronosequence (Fig. 5 & 6). However, mean LAI and FPAR values decreased from the C4 to C5 products across the chronosequence (Fig. 9). The mean C5 FPAR values decreased by 21% and 9% compared to the C4 and C4.1 products, respectively. The C4 LAI product averaged 3.85 m^2 m^{-2} across sites, while the C5 LAI product averaged 2.63 m^2 m^{-2}, or a 32% decrease. In general, C4 and C5 LAI estimates were in closer agreement for evergreen needleleaf forests (Table 4), while the largest differences were observed for the deciduous and mixed sites (i.e. 2003–1964 burns). In addition, the C5 LAI and FPAR products typically displayed smaller variability in the retrieved values compared to the previous C4 (C4.1 for FPAR) products (Figs. 8 & 9), which was likely related to the larger number of high-quality algorithm retrievals in the C5 products (Fig. 4).

4. Discussion

Several studies have examined the spatial accuracy and/or temporal accuracy of the previous collections of the MODIS LAI and FPAR products (e.g. Chasmer et al., 2008; Chen et al., 2005; Cohen et al., 2006; Fensholt et al., 2004; Huemmrich et al., 2005; Pisek & Chen, 2007; Privette et al., 2002; Steinberg et al., 2006). These studies have provided valuable information on the spatial and temporal consistency of the MODIS LAI/FPAR products for various biomes and highlighted numerous opportunities to improve the algorithm (Yang et al., 2006b).

Only a few studies have examined the accuracy of MODIS LAI and/or FPAR seasonal trajectories (Ahl et al., 2006; Fensholt et al., 2004; Huemmrich et al., 2005; Privette et al., 2002; Steinberg et al., 2006), while fewer studies have provided an evaluation of the temporal and spatial accuracy of both the MODIS LAI and FPAR products concurrently, with field observations at consistent locations (Ahl et al., 2006; Fensholt et al., 2004; Huemmrich et al., 2005; this study). Moreover, for generally open boreal forests, a critical issue in the validation of moderate-resolution data, such as from MODIS, is quantifying the contribution of understory vegetation (Kobayashi et al., 2010; Pisek et al., 2010), which can be significant (Serbin et al., 2009). In this study we provide an assessment of the contribution of understory vegetation on LAI and FPAR parameter retrievals (Table 4) and their observed seasonality (Figs. 5 & 6). Finally, only a small number of studies have examined the performance of the latest C5 products (De Kauwe et al., 2011; Fang et al., 2012; Sea et al., 2011; Shabanov et al., 2005; Steinberg & Goetz, 2009; this study).

Validation studies have illustrated three main factors that can influence the accuracy of MODIS LAI and FPAR retrievals (Yang et al., 2006b): 1) uncertainties in the input landcover data, 2) uncertainties associated with a mismatch between observed and simulated reflectance due to improper look-up table (LUT) parameterization, and 3) uncertainties associated with input surface reflectance. In this section we address issues related to 1 and 2. Particular issues related to surface reflectance quality are important for validation but beyond the scope of this paper.

Improper biome classification within the MODIS LAI/FPAR algorithm can introduce errors up to 20% through the inadequate characterization of vegetation (e.g. vertical heterogeneity, single scattering albedo, and crown and background reflectance ranges), however this error can be smaller if similar biomes (i.e. shrubland versus savannas) are interchanged (Myneni et al., 2002). Many previous validation studies have attributed at least some of the differences between LAI/FPAR observations and MODIS retrievals to the improper biome classification

within the input landcover product (e.g. Cheng et al., 2006; Steinberg et al., 2006; Tan et al., 2005; Yang et al., 2006b). For example, Tan et al. (2005) found that the MODIS C4 algorithm overestimated reference LAI for a cropland site in France, however more favorable results were found after reprocessing the data using the correct biome type. Huemmrich et al. (2005) determined that underestimation of the ground cover fraction in sparse, heterogeneous savanna ecosystems led to an overestimate of FPAR by the MODIS algorithm, although they found a closer agreement with LAI. Steinberg et al. (2006) observed that the areas of more recent fires displayed a higher proportion of forest cover (needle-leaf forests) in the MODIS landcover that was contrary to their observations (and this study, Table 2) of a large decline in tree cover following stand-replacing fire. Standing dead, charred biomass, and a burned bryophyte layer, which are common stand structural properties of recently burned boreal forests (Steinberg et al., 2006, Fig. 3), could lead to this confusion with dark dense needle-leaf forest in the MODIS landcover product.

The previous MODIS C4 LAI/FPAR data overestimated observed values for several of the forests examined in this study (Fig. 8, Table 4), which had improper landcover classification (Table 2) in the MODIS algorithm. This improper classification likely contributed, at least partially, to the differences between MODIS and reference values across the chronosequence (Figs 5, 6 & 8). However, the MODIS C5 LAI/FPAR algorithm utilizes a landcover input based on the previous C4 landcover but expanded to include eight biomes (Shabanov et al., 2005; Yang et al., 2006b). Therefore, the substantial improvement in the C5 data suggests that landcover misclassification was not the primary factor for the differences between observed and MODIS LAI and FPAR, especially for the deciduous sites. The improved agreement is likely attributable to other changes, such as the improved LUTs (Shabanov et al., 2005). Moreover, the current C5 landcover product still does not capture the recent burn (Fig. 1, Table 2) which may be due to the temporal period chosen for classification and the methods used to minimize large inter-annual changes in landcover (Friedl et al., 2010). Therefore, landcover will continue to contribute to the differences between observed and MODIS values in future collections, even if an updated landcover product is used, if large-scale disturbances are not properly characterized. This could be an important consideration for the fire-prone boreal forest biome.

The MODIS C4 LAI product greatly over-estimated the LAI of boreal deciduous broadleaf forests (Abuelgasim et al., 2006; Chen et al., 2005; this study). However, the C5 LAI product displayed an overall increase in retrieval accuracy, particularly for broadleaf deciduous forests (Fig. 8, Table 4). This result is consistent with the reduction in retrieval anomalies for dense broadleaf vegetation, which arise from the generally compact and saturated spectral space observed for broadleaf forests (Shabanov et al., 2005; Yang et al., 2006b). The improved C5 product was achieved by utilizing improved look-up table values for saturated conditions (Shabanov et al., 2005). In addition, our results show that the variability in MODIS values decreased at each site in the C5 data, particularly for the broadleaf forests (e.g. 1994, 1989, 1981), which may also be related to the decreased mismatch between observed and simulated red and NIR reflectance values (through the new RTM simulations) and the development of separate sets of LUTs for deciduous broadleaf and conifer forests (Shabanov et al., 2005; Yang et al., 2006b). The last change in the MODIS LAI/FPAR algorithm accounts for the significant differences in spectral properties between these distinct biome classes and growth forms, yielding a lower degree of disagreement between expected and observed MODIS reflectance values.

In contrast with broadleaf forests, the MODIS C4 (e.g. Chen et al., 2005) and C5 LAI products commonly underestimated the LAI of mature conifer forests (Figs. 6 & 8, Table 4). On the other hand, Cohen et al. (2006) found that MODIS C4 LAI generally overestimated Landsat-based LAI reference maps at the northern old black spruce site (NOBS, designated 1850 burn site in this study) by as much as a factor 2 throughout the growing season. However, the unstable peak MODIS LAI values during the growing season (Cohen et al., 2006, this study) may have led to some of the disagreement between MODIS and previous Landsat-based estimates; the validation results are dependent on the temporal period when the comparisons are made. This suggests the importance of repeated measurements during the growing season in order to better represent the uncertainty in MODIS LAI/FPAR.

Overall, MODIS captured the seasonality of both FPAR (Fig. 5) and LAI (Fig. 6) across the chronosequence. In most cases MODIS C5 FPAR fell within the variability of in situ $FPAR_T$ observed along the measurement transects (Fig. 5) and followed the temporal evolution of the LI-191SA FPAR data (Fig. 5, Table 3). Species composition, structure, and topography all effect vegetation phenology, which is evident in the distinct differences between the deciduous and conifer canopies (Figs. 5 & 6) of the early to mid-successional boreal forests (Serbin et al., 2009; Steinberg et al., 2006). For example, Steinberg et al. (2006) found that the MODIS C4 data product generally captured the seasonality of observed FPAR within post-fire boreal deciduous forests using an automated intercepted PAR system similar to this study but that MODIS generally overestimated the magnitude FPAR in all but the oldest, black spruce dominated sites. We observed a similar overestimation of FPAR by the C4 data but found that the C5 data were associated more closely with in situ measurements (Figs. 5 & 8, Table 4).

Another potential source of mismatch that could account for a small portion of the disparity observed between the MODIS and in situ FPAR data, particularly in the young sites (2003–1989), is related to the way FPAR was measured in this study. MODIS FPAR is derived from estimates of canopy spectral absorption of radiation averaged over the PAR wavelengths (Knyazikhin et al., 1998; Shabanov et al., 2003). Our field measurements of FPAR do not quantify PAR absorption or reflection and include interception by non-photosynthetic material (i.e. stems, branches). However, the differences between FPAR and FIPAR (measured in this study) are generally small (<5%) in moderately sparse to mature canopies (Chen et al., 2006; Gower et al., 1999; Huemmrich et al., 2005). Moreover, FIPAR is a relatively good proxy of FPAR for most vegetation conditions (Gobron et al., 2006). Therefore, we conclude that this difference is not a major contributing factor to the differences between field and MODIS FPAR.

4.1. Seasonal boreal reflectance and the influence of the understory

Canopy phenology is a widely used landscape indicator in climate change studies because it is sensitive to environmental factors, and it is closely linked to the CO_2 and H_2O exchanges between terrestrial ecosystems and the atmosphere (Richardson et al., 2010). The largest seasonal changes in LAI and FPAR (65% and 48%, respectively) were observed for the early successional deciduous/mixed sites (2003–1964) while the older (1930 and 1850 burn sites) conifer-dominated forests exhibited only minor seasonal changes (~6 to 14%) in LAI and FPA, which was attributed primarily to understory vegetation dynamics (Serbin et al., 2009).

MODIS captured the seasonal dynamics of LAI and FPAR reasonably well for the deciduous and mixed sites (Figs. 5 and 6). However, MODIS LAI and FPAR had almost a threefold greater seasonal variation (63% vs. 22%) than in situ values for the conifer-dominated sites (Figs. 5 & 6, Table 3). On average, black spruce trees at the BOREAS northern and southern study areas have an average leaf turnover (total foliage mass/new foliage mass) of approximately 12 years (Gower et al., 1997), which relates to a 12% seasonal variation in LAI for a black spruce overstory canopy. Chen (1996) indicated that variations in the overstory LAI are expected to be about 10 to 30% and effective LAI (on which our LAI values are based) is less than 5%. Winter (February to April) MODIS LAI values for the 1930 and 1850 burns averaged 1.5 (ranging between 0.1 and 2.2 $m^2\ m^{-2}$) and mid-summer values were 4.0 $m^2\ m^{-2}$.

Therefore, the MODIS LAI for these conifer sites should range from ~3.5 to 4.5 m^2 m^{-2} during winter months based on previous research (Chen, 1996; Gower et al., 1997; Serbin et al., 2009).

The uncharacteristic seasonality of the MODIS LAI may be related to a combination of poor-illumination conditions (e.g. elongated shadowing), extreme sun-sensor geometry, and a higher snow and cloud cover during winter periods which results in the subsequent increased use of the backup algorithm or otherwise high retrieval uncertainty (Yang et al., 2006b, Fig. 4). Collectively, these factors influence the signal to noise ratio and make use of remote sensing to detect intra- and inter-annual leaf phenology extremely challenging or unlikely — at least with current technologies and analyses for evergreen conifers with long-lived needles. These challenges emphasize the need for extensive field measurements to evaluate MODIS LAI/FPAR products in order to properly characterize the uncertainty in these products. This will aid in the assimilation of these products for parameterizing the biophysical component of terrestrial ecosystem process models (Quaife et al., 2008).

Seasonal variation in the understory vegetation were large (42–79%) across sampling transects (Serbin et al., 2009) and played an important role in the resulting seasonality observed in the MODIS reflectance and LAI/FPAR data. This is consistent with Ahl et al. (2006) who found that the asymmetric phenology between overstory vegetation and understory vegetation significantly influenced the phenological patterns observed by MODIS over a temperate deciduous forests in northern Wisconsin. Furthermore, the rapid recovery of leaf area in recently burned vegetation has been observed for large areas of boreal forest (e.g. Goetz et al., 2006; Hicke et al., 2003; this study). The accumulation of new foliage of the deciduous shrub, forb, and bryophyte layers (Bond-Lamberty & Gower, 2007; Bond-Lamberty et al., 2002; Serbin et al., 2009) likely all contributed to the intra-annual signal observed in the MODIS data across the chronosequence.

The correlation of in situ understory LAI and FPAR with MODIS was relatively high for the conifer sites, suggesting that this vegetation stratum strongly affected the observed seasonality of MODIS reflectance at these sites. Although, the overstory LAI of black spruce stands is relatively constant throughout the year (Figs. 5 & 6; Gower et al., 1997; Serbin et al., 2009), the openness of the canopy allows for understory and ground cover vegetation to contribute to the overall reflectance signal (Miller et al., 1997). Our results emphasize the need to account for the contribution of the understory vegetation to the overall spectral reflectance properties in boreal forests in order to better attribute the observed changes in MODIS reflectance across forests of differing ages, species composition, seasonality, and edaphic conditions.

5. Summary and conclusions

The spatial and temporal characteristics of the MODIS MOD15A2 biophysical (LAI/FPAR) products were analyzed for a boreal forest wildfire chronosequence in northern Manitoba, Canada. The results of this study illustrate that the MODIS LAI and FPAR products both generally describe the seasonality of LAI and FPAR for these post-fire boreal forests. However, we observed small to moderate disparities between MODIS and in situ measurements, although these differences have decreased substantially in the current MODIS collection (C5) compared to the previous products (C4). The improvements appear to be related primarily to changes in the algorithm behind the radiative transfer simulations and resultant look-up table (LUT) values (Shabanov et al., 2005), as opposed to other potential reasons such as the changes to the input landcover product (i.e. inclusion of eight rather than six biome classifications). Key findings of this study are:

- The updated MODIS C5 LAI/FPAR product has significantly increased the number of growing season high-quality retrievals compared to the previous C4 data.
- Early and late season retrievals still appear to be impacted by snow and poor sun-sensor geometry, which may be an issue that cannot be overcome.
- Overall, the C5 LAI and FPAR products show much higher spatial and temporal correlation with in situ values over the C4 data. However, the new products (C5) still overestimate and underestimate the LAI and FPAR at the youngest and oldest sites, respectively, and display unreasonable seasonality for evergreen needleleaf forests.
- Improvements in the characterization of foliage clumping at stand and landscape scales, as well as the increased ability to simulate the variability of reflectance within broadleaf forests, are likely the primary reasons for the increased LAI/FPAR accuracy and reduction in within-site variability. However, the change in algorithm biome classes as well as the separation of deciduous and evergreen broadleaf forest look-up tables also likely contributed.
- Understory vegetation comprises a large portion of the seasonal signal observed by MODIS surface reflectance and LAI/FPAR retrievals. Therefore, it is important to characterize the full canopy LAI in order to properly validate these products in boreal forests of North America.
- Large, stand replacing disturbances need to be accounted for in the MODIS landcover product in order to properly parameterize future versions of the MODIS MOD15A2 algorithm and capture the dynamic changes in vegetation composition across boreal forests. While we observed that landcover did not contribute a large proportion of the error in LAI/FPAR retrievals in this study, further improvements in accuracy could be achieved over recently burned sites by accounting for the resultant changes in composition and canopy structure.

Acknowledgments

The National Aeronautics and Space Administration (NASA) supported this research under grant number NNG04GL26G, awarded to S.T. Gower and D.E. Ahl. We are enormously grateful to Shelley Schmidt, Jennifer Smith, Jessica Nelson-Urban, Chris Kniffen, and Kevin Wilson for their dedicated help and willingness to hike through difficult terrain, often in the dark. We graciously thank Phil Townsend for supporting S.P.S in the writing of this article and the assistance of Jeff Morisette and Jaime Nickeson in accessing the ASTER data archive, helping to coordinate validation activities, and for helpful discussions. We are indebted to Bruce Holmes of the Manitoba Conservation Department (MCD) for advice and necessary permits. We are additionally indebted to the Nisichawayasihk First Nation for permission to collect data on tribal land. Finally, we thank three anonymous reviewers for their helpful comments that greatly improved the earlier versions of the manuscript.

Appendix A. Supplementary data

Supplementary data associated with this article can be found in the online version, at http://dx.doi.org/10.1016/j.rse.2013.01.022. This information contains a KML file showing the field plot locations within each forest site comprising the wildfire chronosequence.

References

Abrams, M., Hook, S., & Ramachandran, B. (2002). *ASTER user handbook version 2* (pp. 135). Jet Propulsion Laboratory/California Institute of Technology (CIT).

Abuelgasim, A. A., Fernandes, R. A., & Leblanc, S. G. (2006). Evaluation of national and global LAI products derived from optical remote sensing instruments over Canada. *IEEE Transactions on Geoscience and Remote Sensing*, *44*, 1872–1884.

ACIA (2004). Impacts of a warming Arctic. *Synthesis report of the Arctic Climate Impacts Assessment* (pp. 140). Cambridge, U.KCambridge University Press.

Ahl, D. E., Gower, S. T., Burrows, S. N., Shabanov, N. V., Myneni, R. B., & Knyazikhin, Y. (2006). Monitoring spring canopy phenology of a deciduous broadleaf forest using MODIS. *Remote Sensing of Environment*, *104*, 88–95.

Amiro, B. D. (2001). Paired-tower measurements of carbon and energy fluxes following disturbance in the boreal forest. *Global Change Biology*, *7*, 253–268.

Amiro, B. D., Barr, A. G., Black, T. A., Iwashita, H., Kljun, N., McCaughey, J. H., et al. (2006). Carbon, energy and water fluxes at mature and disturbed forest sites, Saskatchewan, Canada. *Agricultural and Forest Meteorology*, *136*, 237–251.

Angert, A., Biraud, S., Bonfils, C., Henning, C. C., Buermann, W., Pinzon, J., et al. (2005). Drier summers cancel out the CO_2 uptake enhancement induced by warmer springs. *Proceedings of the National Academy of Sciences (PNAS) of the United States of America*, *102*, 10823–10827.

Barr, A. G., Black, T. A., Hogg, E. H., Griffis, T. J., Morgenstern, K., Kljun, N., et al. (2007). Climatic controls on the carbon and water balances of a boreal aspen forest, 1994–2003. *Global Change Biology*, *13*, 561–576.

Barr, A. G., Black, T. A., Hogg, E. H., Kljun, N., Morgenstern, K., & Nesic, Z. (2004). Inter-annual variability in the leaf area index of a boreal aspen-hazelnut forest in relation to net ecosystem production. *Agricultural and Forest Meteorology*, *126*, 237–255.

Bonan, G. B. (1993). Importance of leaf area index and forest type when estimating photosynthesis in boreal forests. *Remote Sensing of Environment*, *43*, 303–314.

Bond-Lamberty, B., & Gower, S. T. (2007). Estimation of stand-level leaf area for boreal bryophytes. *Oecologia*, *151*, 584–592.

Bond-Lamberty, B., Peckham, S. D., Ahl, D. E., & Gower, S. T. (2007). Fire as the dominant driver of central Canadian boreal forest carbon balance. *Nature*, *450*, 89–93.

Bond-Lamberty, B., Wang, C. K., & Gower, S. T. (2004). Net primary production and net ecosystem production of a boreal black spruce wildfire chronosequence. *Global Change Biology*, *10*, 473–487.

Bond-Lamberty, B., Wang, C., Gower, S. T., & Norman, J. (2002). Leaf area dynamics of a boreal black spruce fire chronosequence. *Tree Physiology*, *22*, 993–1001.

Chasmer, L., Hopkinson, C., Treitz, P., McCaughey, H., Barr, A., & Black, A. (2008). A LiDAR-based hierarchical approach for assessing MODIS fPAR. *Remote Sensing of Environment*, *112*, 4344–4357.

Chen, J. M. (1996). Optically-based methods for measuring seasonal variation of leaf area index in boreal conifer stands. *Agricultural and Forest Meteorology*, *80*, 135–163.

Chen, J. M., & Cihlar, J. (1995). Quantifying the effect of canopy architecture on optical measurements of leaf-area index using 2 gap size analysis-methods. *IEEE Transactions on Geoscience and Remote Sensing*, *33*, 777–787.

Chen, J. M., Govind, A., Sonnentag, O., Zhang, Y. Q., Barr, A., & Amiro, B. (2006). Leaf area index measurements at Fluxnet-Canada forest sites. *Agricultural and Forest Meteorology*, *140*, 257–268.

Chen, J. M., Rich, P. M., Gower, S. T., Norman, J. M., & Plummer, S. (1997). Leaf area index of boreal forests: Theory, techniques, and measurements. *Journal of Geophysical Research-Atmospheres*, *102*, 29429–29443.

Chen, X., Vierling, L., Deering, D., & Conley, A. (2005). Monitoring boreal forest leaf area index across a Siberian burn chronosequence: A MODIS validation study. *International Journal of Remote Sensing*, *26*, 5433–5451.

Cheng, Y. F., Gamon, J. A., Fuentes, D. A., Mao, Z. Y., Sims, D. A., Qiu, H. L., et al. (2006). A multi-scale analysis of dynamic optical signals in a Southern California chaparral ecosystem: A comparison of field, AVIRIS and MODIS data. *Remote Sensing of Environment*, *103*, 369–378.

Cohen, W. B., Maiersperger, T. K., Gower, S. T., & Turner, D. P. (2003). An improved strategy for regression of biophysical variables and Landsat ETM + data. *Remote Sensing of Environment*, *84*, 561–571.

Cohen, W. B., Maiersperger, T. K., Turner, D. P., Ritts, W. D., Pflugmacher, D., Kennedy, R. E., et al. (2006). MODIS land cover and LAI collection 4 product quality across nine sites in the Western Hemisphere. *IEEE Transactions on Geoscience and Remote Sensing*, *44*, 1843–1857.

Cox, P. M., Betts, R. A., Jones, C. D., Spall, S. A., & Totterdell, I. J. (2000). Acceleration of Global warming due to carbon-cycle feedbacks in a coupled climate model. *Nature*, *408*, 184–187.

de Beurs, K. M., & Henebry, G. M. (2010). A land surface phenology assessment of the northern polar regions using MODIS reflectance time series. *Canadian Journal of Remote Sensing*, *36*, S87–S110.

De Kauwe, M. G., Disney, M. I., Quaife, T., Lewis, P., & Williams, M. (2011). An assessment of the MODIS collection 5 leaf area index product for a region of mixed coniferous forest. *Remote Sensing of Environment*, *115*, 767–780.

Fang, H., Wei, S., & Liang, S. (2012). Validation of MODIS and CYCLOPES LAI products using global field measurement data. *Remote Sensing of Environment*, *119*, 43–54.

Fensholt, R., Sandholt, I., & Rasmussen, M. S. (2004). Evaluation of MODIS LAI, fAPAR and the relation between fAPAR and NDVI in a semi-arid environment using in situ measurements. *Remote Sensing of Environment*, *91*, 490–507.

Flannigan, M. D., Logan, K. A., Amiro, B. D., Skinner, W. R., & Stocks, B. J. (2005). Future area burned in Canada. *Climatic Change*, *72*, 1–16.

Friedl, M. A., McIver, D. K., Hodges, J. C. F., Zhang, X. Y., Muchoney, D., Strahler, A. H., et al. (2002). Global land cover mapping from MODIS: Algorithms and early results. *Remote Sensing of Environment*, *83*, 287–302.

Friedl, M. A., Sulla-Menashe, D., Tan, B., Schneider, A., Ramankutty, N., Sibley, A., et al. (2010). MODIS Collection 5 global land cover: Algorithm refinements and characterization of new datasets. *Remote Sensing of Environment*, *114*, 168–182.

Garrigues, S., Allard, D., Baret, F., & Weiss, M. (2006). Influence of landscape spatial heterogeneity on the non-linear estimation of leaf area index from moderate spatial resolution remote sensing data. *Remote Sensing of Environment*, *105*, 286–298.

Garrigues, S., Lacaze, R., Baret, F., Morisette, J. T., Weiss, M., Nickeson, J. E., et al. (2008). Validation and intercomparison of global leaf area index products derived from remote sensing data. *Journal of Geophysical Research-Biogeosciences*, *113*.

Geladi, P., & Kowalski, B. R. (1986). Partial least-squares regression — A tutorial. *Analytica Chimica Acta*, *185*, 1–17.

Gillett, N. P., Weaver, A. J., Zwiers, F. W., & Flannigan, M. D. (2004). Detecting the effect of climate change on Canadian forest fires. *Geophysical Research Letters*, *31*.

Gobron, N., Pinty, B., Aussedat, O., Chen, J. M., Cohen, W. B., Fensholt, R., et al. (2006). Evaluation of fraction of absorbed photosynthetically active radiation products for different canopy radiation transfer regimes: Methodology and results using Joint Research Center products derived from SeaWiFS against ground-based estimations. *Journal of Geophysical Research-Atmospheres*, *111*.

Goetz, S. J., Bunn, A. G., Fiske, G. J., & Houghton, R. A. (2005). Satellite-observed photosynthetic trends across boreal North America associated with climate and fire disturbance. *Proceedings of the National Academy of Sciences of the United States of America*, *102*, 13521–13525.

Goetz, S. J., Fiske, G. J., & Bunn, A. G. (2006). Using satellite time-series data sets to analyze fire disturbance and forest recovery across Canada. *Remote Sensing of Environment*, *101*, 352–365.

Goulden, M. L., McMillan, A. M. S., Winston, G. C., Rocha, A. V., Manies, K. L., Harden, J. W., et al. (2011). Patterns of NPP, GPP, respiration, and NEP during boreal forest succession. *Global Change Biology*, *17*(2), 855–871.

Gower, S. T., Kucharik, C. J., & Norman, J. M. (1999). Direct and indirect estimation of Leaf Area Index, F(Apar), and net primary production of terrestrial ecosystems. *Remote Sensing of Environment*, *70*, 29–51.

Gower, S. T., & Richards, J. H. (1991). Larches: Deciduous conifers in an evergreen world. *Bioscience*, *40*, 818–826.

Gower, S. T., Vogel, J. G., Norman, J. M., Kucharik, C. J., Steele, S. J., & Stow, T. K. (1997). Carbon distribution and aboveground net primary production in aspen, jack pine, and black spruce stands in Saskatchewan and Manitoba, Canada. *Journal of Geophysical Research-Atmospheres*, *102*, 29029–29041.

Hansen, J., Sato, M., Ruedy, R., Lo, K., Lea, D. W., & Medina-Elizade, M. (2006). Global temperature change. *Proceedings of the National Academy of Sciences of the United States of America*, *103*, 14288–14293.

Hicke, J. A., Asner, G. P., Kasischke, E. S., French, N. H. F., Randerson, J. T., Collatz, G. J., et al. (2003). Postfire response of North American boreal forest net primary productivity analyzed with satellite observations. *Global Change Biology*, *9*, 1145–1157.

Hofmann, D. J., Butler, J. H., Dlugokencky, E. J., Elkins, J. W., Masarie, K., Montzka, S. A., et al. (2006). The role of carbon dioxide in climate forcing from 1979 to 2004: Introduction of the Annual Greenhouse Gas Index. *Tellus Series B: Chemical and Physical Meteorology*, *58*, 614–619.

Huang, D., Yang, W. Z., Tan, B., Rautiainen, M., Zhang, P., Hu, J. N., et al. (2006). The Importance of measurement errors for deriving accurate reference leaf area index maps for validation of moderate-resolution satellite LAI products. *IEEE Transactions on Geoscience and Remote Sensing*, *44*, 1866–1871.

Huang, D., Knyazikhin, Y., Dickinson, R. E., Rautiainen, M., Stenberg, P., Disney, M., et al. (2007). Canopy spectral invariants for remote sensing and model applications. *Remote Sensing of Environment*, *106*, 106–122.

Huemmrich, K. F., Privette, J. L., Mukelabai, M., Myneni, R. B., & Knyazikhin, Y. (2005). Time-series validation of MODIS land biophysical products in a Kalahari woodland, Africa. *International Journal of Remote Sensing*, *26*, 4381–4398.

IPCC (2007). *Climate change 2007: The physical science basis, contribution of working group I to the fourth assessment report of the IPCC*. Cambridge, UKCambridge University Press.

Johnstone, J. F., & Chapin, F. S. (2006). Fire interval effects on successional trajectory in boreal forests of northwest Canada. *Ecosystems*, *9*, 268–277.

Johnstone, J. F., & Kasischke, E. S. (2005). Stand-level effects of soil burn severity on postfire regeneration in a recently burned black spruce forest. *Canadian Journal of Forest Research*, *35*, 2151–2163.

Kasischke, E. S., & Turetsky, M. R. (2006). Recent changes in the fire regime across the North American boreal region — Spatial and temporal patterns of burning across Canada and Alaska. *Geophysical Research Letters*, *33*.

Keeling, C. D., Chin, J. F. S., & Whorf, T. P. (1996). Increased activity of northern vegetation inferred from atmospheric CO_2 measurements. *Nature*, *382*, 146–149.

Knyazikhin, Y., Martonchik, J. V., Myneni, R. B., Diner, D. J., & Running, S. W. (1998). Synergistic algorithm for estimating vegetation canopy leaf area index and fraction of absorbed photosynthetically active radiation from MODIS and MISR data. *Journal of Geophysical Research-Atmospheres*, *103*, 32257–32275.

Kobayashi, H., Delbart, N., Suzuki, R., & Kushida, K. (2010). A satellite-based method for monitoring seasonality in the overstory leaf area index of Siberian larch forest. *Journal of Geophysical Research-Biogeosciences*, *115*.

Kucharik, C. J., Norman, J. M., & Gower, S. T. (1999). Characterization of radiation regimes in nonrandom forest canopies: Theory, measurements, and a simplified modeling approach. *Tree Physiology*, *19*, 695–706.

Kurz, W. A., Stinson, G., & Rampley, G. (2008). Could increased boreal forest ecosystem productivity offset carbon losses from increased disturbances? *Philosophical Transactions of the Royal Society B-Biological Sciences*, *363*, 2261–2269.

Lacis, A. A., Schmidt, G. A., Rind, D., & Ruedy, R. A. (2010). Atmospheric CO_2: Principal control knob governing Earth's temperature. *Science*, *330*, 356–359.

Lucht, W., Prentice, I. C., Myneni, R. B., Sitch, S., Friedlingstein, P., Cramer, W., et al. (2002). Climatic control of the high-latitude vegetation greening trend and Pinatubo effect. *Science*, *296*, 1687–1689.

Mcguire, A. D., Wirth, C., Apps, M., Beringer, J., Clein, J., Epstein, H., et al. (2002). Environmental variation, vegetation distribution, carbon dynamics and water/energy exchange at high latitudes. *Journal of Vegetation Science*, *13*, 301–314.

Miller, J. R., White, H. P., Chen, J. M., Peddle, D. R., Mcdermid, G., Fournier, R. A., et al. (1997). Seasonal change in understory reflectance of boreal forests and influence on canopy vegetation indices. *Journal of Geophysical Research-Atmospheres*, *102*, 29475–29482.

Morisette, J. T., Baret, F., Privette, J. L., Myneni, R. B., Nickeson, J. E., Garrigues, S., et al. (2006). Validation of global moderate-resolution LAI products: A framework proposed within the CEOS Land Product Validation subgroup. *IEEE Transactions on Geoscience and Remote Sensing*, *44*, 1804–1817.

Myneni, R. B., Hoffman, S., Knyazikhin, Y., Privette, J. L., Glassy, J., Tian, Y., et al. (2002). Global products of vegetation leaf area and fraction absorbed par from year one of MODIS Data. *Remote Sensing of Environment*, *83*, 214–231.

Myneni, R. B., Keeling, C. D., Tucker, C. J., Asrar, G., & Nemani, R. R. (1997). Increased plant growth in the northern high latitudes from 1981 to 1991. *Nature*, *386*, 698–702.

Peckham, S. D., Ahl, D. E., Serbin, S. P., & Gower, S. T. (2008). Fire-induced changes in green-up and leaf maturity of the Canadian boreal forest. *Remote Sensing of Environment*, *112*, 3594–3603.

Piao, S. L., Ciais, P., Friedlingstein, P., Peylin, P., Reichstein, M., Luyssaert, S., et al. (2008). Net carbon dioxide losses of northern ecosystems in response to autumn warming. *Nature*, *451*.

Piao, S., Friedlingstein, P., Ciais, P., Viovy, N., & Demarty, J. (2007). Growing season extension and its impact on terrestrial carbon cycle in the Northern Hemisphere over the past 2 decades. *Global Biogeochemical Cycles*, *21*, GB3018.

Pisek, J., & Chen, J. M. (2007). Comparison and validation of MODIS and VEGETATION global LAI products over four BigFoot sites in North America. *Remote Sensing of Environment*, *109*, 81–94.

Pisek, J., Chen, J. M., Alikas, K., & Deng, F. (2010). Impacts of including forest understory brightness and foliage clumping information from multiangular measurements on leaf area index mapping over North America. *Journal of Geophysical Research-Biogeosciences*, *115*.

Privette, J. L., Myneni, R. B., Knyazikhin, Y., Mukelabai, M., Roberts, G., Tian, Y., et al. (2002). Early spatial and temporal validation of MODIS LAI product in the Southern Africa Kalahari. *Remote Sensing of Environment*, *83*, 232–243.

Quaife, T., Lewis, P., De Kauwe, M., Williams, M., Law, B. E., Disney, M., et al. (2008). Assimilating canopy reflectance data into an ecosystem model with an Ensemble Kalman Filter. *Remote Sensing of Environment*, *112*, 1347–1364.

Randerson, J. T., Field, C. B., Fung, I. Y., & Tans, P. P. (1999). Increases in early season ecosystem uptake explain recent changes in the seasonal cycle of atmospheric CO_2 at high northern latitudes. *Geophysical Research Letters*, *26*, 2765–2768.

Raupach, M. R., Marland, G., Ciais, P., Le Quere, C., Canadell, J. G., Klepper, G., et al. (2007). Global and regional drivers of accelerating CO_2 emissions. *Proceedings of the National Academy of Sciences of the United States of America*, *104*, 10288–10293.

Richardson, A. D., Black, T. A., Ciais, P., Delbart, N., Friedl, M. A., Gobron, N., et al. (2010). Influence of spring and autumn phenological transitions on forest ecosystem productivity. *Philosophical Transactions of the Royal Society B-Biological Sciences*, *365*, 3227–3246.

Running, S. W., Nemani, R. R., Heinsch, F. A., Zhao, M. S., Reeves, M., & Hashimoto, H. (2004). A continuous satellite-derived measure of global terrestrial primary production. *Bioscience*, *54*, 547–560.

Sanderson, M. G., Hemming, D. L., & Betts, R. A. (2011). Regional temperature and precipitation changes under high-end (≥4 °C) global warming. *Philosophical Transactions of the Royal Society A-Mathematical Physical and Engineering Sciences*, *369*, 85–98.

Sea, W. B., Choler, P., Beringer, J., Weinmann, R. A., Hutley, L. B., & Leuning, R. (2011). Documenting improvement in leaf area index estimates from MODIS using hemispherical photos for Australian savannas. *Agricultural and Forest Meteorology*, *151*, 1453–1461.

Sellers, P. J., Dickinson, R. E., Randall, D. A., Betts, A. K., Hall, F. G., Berry, J. A., et al. (1997a). Modeling the exchanges of energy, water, and carbon between continents and the atmosphere. *Science*, *275*, 502–509.

Sellers, P. J., Hall, F. G., Kelly, R. D., Black, A., Baldocchi, D., Berry, J., et al. (1997b). BOREAS in 1997: Experiment overview, scientific results, and future directions. *Journal of Geophysical Research-Atmospheres*, *102*, 28731–28769.

Serbin, S. P., Dillaway, D. N., Kruger, E. L., & Townsend, P. A. (2012). Leaf optical properties reflect variation in photosynthetic metabolism and its sensitivity to temperature. *Journal of Experimental Botany*, *63*(1), 489–502.

Serbin, S. P., Gower, S. T., & Ahl, D. E. (2009). Canopy dynamics and phenology of a boreal black spruce wildfire chronosequence. *Agricultural and Forest Meteorology*, *149*, 187–204.

Shabanov, N. V., Huang, D., Yang, W. Z., Tan, B., Knyazikhin, Y., Myneni, R. B., et al. (2005). Analysis and optimization of the MODIS leaf area index algorithm retrievals over broadleaf forests. *IEEE Transactions on Geoscience and Remote Sensing*, *43*, 1855–1865.

Shabanov, N. V., Wang, Y., Buermann, W., Dong, J., Hoffman, S., Smith, G. R., et al. (2003). Effect of foliage spatial heterogeneity in the MODIS LAI and FPAR algorithm over broadleaf forests. *Remote Sensing of Environment*, *85*, 410–423.

Shabanov, N. V., Zhou, L. M., Knyazikhin, Y., Myneni, R. B., & Tucker, C. J. (2002). Analysis of interannual changes in northern vegetation activity observed in AVHRR data from 1981 to 1994. *IEEE Transactions on Geoscience and Remote Sensing*, *40*, 115–130.

Smith, M. L., Ollinger, S. V., Martin, M. E., Aber, J. D., Hallett, R. A., & Goodale, C. L. (2002). Direct estimation of aboveground forest productivity through hyperspectral remote sensing of canopy nitrogen. *Ecological Applications*, *12*, 1286–1302.

Steinberg, D. C., & Goetz, S. (2009). Assessment and extension of the MODIS FPAR products in temperate forests of the eastern United States. *International Journal of Remote Sensing*, *30*, 169–187.

Steinberg, D. C., Goetz, S. J., & Hyer, E. J. (2006). Validation of MODIS F_{PAR} products in boreal forests of Alaska. *IEEE Transactions on Geoscience and Remote Sensing*, *44*, 1818–1828.

Stocks, B. J., Fosberg, M. A., Lynham, T. J., Mearns, L., Wotton, B. M., Yang, Q., et al. (1998). Climate change and forest fire potential in Russian and Canadian boreal forests. *Climatic Change*, *38*, 1–13.

Stocks, B. J., Mason, J. A., Todd, J. B., Bosch, E. M., Wotton, B. M., Amiro, D., et al. (2003). Large forest fires in Canada, 1959–1997. *Journal of Geophysical Research*, *108*(5–1), 5–12.

Tan, B., Hu, J. N., Zhang, P., Huang, D., Shabanov, N., Weiss, M., et al. (2005). Validation of moderate resolution imaging spectroradiometer leaf area index product in croplands of Alpilles, France. *Journal of Geophysical Research-Atmospheres*, *110*, 16.

Tarnocai, C., Canadell, J. G., Schuur, E. A. G., Kuhry, P., Mazhitova, G., & Zimov, S. (2009). Soil organic carbon pools in the northern circumpolar permafrost region. *Global Biogeochemical Cycles*, *23*.

Townsend, P. A., Foster, J. R., Chastain, R. A., & Currie, W. S. (2003). Application of imaging spectroscopy to mapping canopy nitrogen in the forests of the central Appalachian Mountains using Hyperion and AVIRIS. *IEEE Transactions on Geoscience and Remote Sensing*, *41*, 1347–1354.

Turetsky, M. R., Kane, E. S., Harden, J. W., Ottmar, R. D., Manies, K. L., Hoy, E., et al. (2011). Recent acceleration of biomass burning and carbon losses in Alaskan forests and peatlands. *Nature Geoscience*, *4*, 27–31.

Vermote, E. F., ElSaleous, N., Justice, C. O., Kaufman, Y. J., Privette, J. L., Remer, L., et al. (1997). Atmospheric correction of visible to middle-infrared EOS-MODIS data over land surfaces: Background, operational algorithm and validation. *Journal of Geophysical Research-Atmospheres*, *102*, 17131–17141.

Viereck, L. A., Dyrness, C. T., Vancleve, K., & Foote, M. J. (1983). Vegetation, soils, and forest productivity in selected forest types in interior Alaska. *Canadian Journal of Forest Research*, *13*, 703.

Wang, Y. J., Woodcock, C. E., Buermann, W., Stenberg, P., Voipio, P., Smolander, H., et al. (2004). Evaluation of the MODIS LAI algorithm at a coniferous forest site in Finland. *Remote Sensing of Environment*, *91*, 114–127.

Wold, S., Ruhe, A., Wold, H., & Dunn, W. J. (1984). The collinearity problem in linear-regression — The partial least-squares (PLS) approach to generalized inverses. *SIAM Journal on Scientific and Statistical Computing*, *5*, 735–743.

Wolter, P. T., Townsend, P. A., Sturtevant, B. R., & Kingdon, C. C. (2008). Remote sensing of the distribution and abundance of host species for spruce budworm in Northern Minnesota and Ontario. *Remote Sensing of Environment*, *112*, 3971–3982.

Yang, W. Z., Huang, D., Tan, B., Stroeve, J. C., Shabanov, N. V., Knyazikhin, Y., et al. (2006a). Analysis of leaf area index and fraction of PAR absorbed by vegetation products from the Terra MODIS sensor: 2000–2005. *IEEE Transactions on Geoscience and Remote Sensing*, *44*, 1829–1842.

Yang, W. Z., Tan, B., Huang, D., Rautiainen, M., Shabanov, N. V., Wang, Y., et al. (2006b). MODIS leaf area index products: From validation to algorithm improvement. *IEEE Transactions on Geoscience and Remote Sensing*, *44*, 1885–1898.